Polar Biology (2022) 45:309–329
https://doi.org/10.1007/s00300-021-02986-2

ORIGINAL PAPER

Postnatal ontogeny of the spine of the Emperor Penguin *Aptenodytes forsteri* (Aves, Sphenisciformes) and modularity of the neck

M. Alejandra Sosa[1,2] · **Carolina Acosta Hospitaleche**[1,3]

Received: 10 June 2021 / Revised: 2 December 2021 / Accepted: 6 December 2021 / Published online: 25 January 2022

Abstract

The Emperor Penguin (*Aptenodytes forsteri*), the largest extant penguin, inhabits exclusively in Antarctica. Little is known about the spine of this species; this work presents a description of the vertebral column of an adult of *A. forsteri*, compared with specimens from different ontogenetic stages (chick, fledgling, and juvenile). We also analyze the regionalization of the spine with a principal component analysis (PCA), and the modularity with an elliptical Fourier analysis, performing a PCA, followed by a linear discriminant analysis on the PC scores. Our results show that the vertebrae are completely ossified in adults, while the suture lines between the different elements are visible in the previous stages and some structures remain cartilaginous. A total of 42/43 vertebrae were counted (13 cervicals, 2 cervicothoracics, 6/7 thoracics, 13 synsacrals, and 8 caudals), and an extra vertebra appears in the thoracic region of one specimen. These regions are already differentiated in fledglings, but not in chicks. Six modules associated with the S-shape of the adult neck were recognized and are represented by different numbers of vertebrae: module 1 (C1), module 2 (C2), module 3 (C3–5), module 4 (C6), module 5 (C7–9) and module 6 (C10–13). Differences in the vertebral configuration in modules 5 and 6 of previous stages were found, where cervical 10 is part of module 5 due to the absence of the *processus ventralis corporis*.

Keywords Cervical modules · Osteology · Vertebral column · Vertebral regions

Introduction

Penguins (Aves, Sphenisciformes) are highly specialized birds for marine life. They present a body with a hydrodynamic shape, short neck, paddle-like forelimbs, and short and caudally positioned hindlimbs (Winkler et al. 2020). The Antarctic *Aptenodytes forsteri* Gray 1844, that reaches 115 cm height and 46 kg weight (Martínez et al. 2020), is the largest species among the living forms.

The Emperor Penguin *A. forsteri* has been the subject of numerous studies (Prévost 1961; Isenmann and Jouventin 1970; Jouventin 1971; Klages 1989; Wienecke and Robertson 1997; Cherel and Kooyman 1998), but only few of them focus on its osteological anatomy (Stephan 1979; Guinard and Marchand 2010; Sosa and Acosta Hospitaleche 2018). In the present contribution, we analyze the spine of *A. forsteri*, taking into account the following aspects: general morphology, postnatal ontogenetic variation, regionalization, and modularity of the cervical portion.

The spine is the part of the axial skeleton that protects the spinal cord, provides support and stability to the entire body, and serves as the origin and insertion of muscles. The spine is divided into regions (Galbusera 2018; Galbusera and Bassani 2019) that, in birds, are named as cervical, thoracic, synsacral, caudal, and pygostyle. The cervical vertebrae have fused or absent ribs (Zusi 1962; Baumel and Witmer 1993). The thoracic ones carry complete ribs, articulating directly or indirectly with the sternum (Baumel and Witmer 1993). Some vertebrae called "transitional" (Fürbringer 1888) or "cervicothoracic" (Newton 1896; Pycraft 1898; Virchow 1931; Zusi 1962; Baumel and Witmer 1993; Jadwiszczak 2014a) carry free ribs (not contacting with the sternum) and exhibit a transitional morphology between the cervical and thoracic vertebrae (Baumel and Witmer 1993). The synsacral region corresponds to the synsacrum, a rigid

✉ M. Alejandra Sosa
alejandrasosa@fcnym.unlp.edu.ar

[1] División Paleontología Vertebrados, Museo de La Plata, Facultad de Ciencias Naturales y Museo, Paseo del Bosque s/n, 1900, La Plata, Buenos Aires, Argentina

[2] UNLP, La Plata, Argentina

[3] CONICET, Buenos Aires, Argentina

structure of ankylosed vertebrae in adults, that incorporates some thoracic, lumbar, sacral, and the most proximal caudal vertebrae (Baumel and Witmer 1993). Finally, the caudal region is subdivided into a portion of free vertebrae and the pygostyle, an element formed by postnatal ankylosis of the last five–nine caudal vertebrae (Baumel 1988; Baumel and Witmer 1993).

The number of vertebrae in penguins differs from 42 vertebrae in *Eudyptes chrysocome*, *Eudyptes chrysolophus*, *Eudyptula minor*, *Pygoscelis papua*, and *Aptenodytes patagonicus* (Watson 1883; Shufeldt 1901; Stephan 1979) to 43 in *Spheniscus demersus*, *Spheniscus magellanicus*, and *Spheniscus mendiculus* (Watson 1883). The cervical region comprises 13 (Watson 1883; Stephan 1979; Guinard and Marchand 2010; Guinard et al. 2010) or 15 vertebrae (sensu Shufeldt 1901 and including the 2 cervicothoracics) depending on the author. Recent approaches consider the cervicothoracic vertebrae as a distinct region (Jadwiszczak 2014a). On the other hand, the thoracic region includes six (Shufeldt 1901) or eight–nine vertebrae (Stephan 1979 and Watson 1883 respectively, due to the inclusion of the cervicothoracics).

The constitution of the synsacrum varies from 12 (Watson 1883, considering the first synsacral vertebra as thoracic) to 14 (Stephan 1979). Depending on the species and the ontogenetic stage, the synsacrum includes from one to three caudal vertebrae (Pycraft 1898). In penguins, it is divided in five segments: thoracic, thoracolumbar, lumbar, sacral, and caudal (Stephan 1979). The thoracic segment comprises a single vertebra with ribs; the thoracolumbar has five vertebrae with wide *processi transversi* (and the last three vertebrae with *processi costale*). The lumbar segment comprises two–three vertebrae without *processi costale*, whereas the sacral has two vertebrae with strong *processi costale*. The caudal segment presents two–three vertebrae morphologically similar to the free caudals (see below).

The caudal region comprises six–seven free vertebrae with well-developed *processi transversi* (Watson 1883; Shufeldt 1901; Stephan 1979) and the pygostyle. The pygostyle is constituted by the fusion of the six–seven last caudal vertebrae (Stephan 1979).

It is worth mentioning here that postnatal variation of the penguin spine was only occasionally evaluated. A complex analysis of the cervical region was made with specimens of different ages (Guinard and Marchand 2010; Guinard et al. 2010), and more recently, the synsacra of juveniles of *Aptenodytes* and *Pygoscelis* were examined with comparative purposes (Jadwiszczak 2014b).

Analyses of modularity in the cervical region of penguins were made by Guinard et al. (2010) following the definition of modules provided by Klingenberg (2002). In this context, a module is considered as a group of elements morphologically similar and identified by a biomechanical function. The number of vertebrae included in each module varies interspecifically. According to that, the cervical region was divided into six portions reflecting the morphologic variations during growth and the neck flexibility in adults (Guinard and Marchand 2010; Guinard et al. 2010).

The first three modules (Mo1, Mo2, Mo3) connect the skull with the rest of the skeleton and contribute to the formation of the most proximal neck curvature. These segments help bring the head back, and rotate it. The fourth module (Mo4) is a transitional zone toward the fifth module (Mo5). It is identified as "mechanical curvature" because the folding of this zone is induced by the preceding and the posterior modules. The sixth module (Mo6) comprises the second cervical curvature and keeps the base of the neck backwards (Guinard et al. 2010).

These modules vary along postnatal ontogeny. In juveniles, the neck does not have a strongly folded S-shape mainly because the *processi articulare craniale* are not completely developed, particularly in the middle zone of the neck (Guinard et al. 2010). The modular configuration changes along ontogenetic growth, probably related to the ecological requirements of each stage. While chicks and juveniles are more terrestrial, adults acquire an eminently marine mode of life. For that reason, the folding of the neck must be more efficient in adults to bring the head closer to the body and thus achieve a hydrodynamic shape (Guinard et al. 2010).

Starting from these premises as the only background in this topic, we characterized each vertebra and the spine regions of *A. forsteri*, highlighting the individual and postnatal ontogenetic variations. The cervical modules in fledgling and adult specimens were also determined, omitting chicks that were too small or un-ossified for this kind of analysis.

Materials and methods

Materials

Skeletons analyzed here are deposited in the collections of the Vertebrate Zoology Department (adult MLP-O-15192, juvenile MLP-O-15035) and the Vertebrate Paleontology Department (adult MLP-478, fledgling MLP-1014, chicks MLP-1010, MLP-1011, MLP-1012, MLP-1013) of the Museo de La Plata, and the Ornithology Section of the Museo Argentino de Ciencias Naturales (adult MACN-OR-8462), Ciudad de Buenos Aires, Argentina. Four specimens were collected on Snow Hill Island (Antarctica) immediately after natural death during the austral summer field trip of 2014 by members of the Instituto Antártico Argentino. Ontogenetic stages concur with Stonehouse (1953).

One of the bodies was preserved in a 70% ethyl alcohol solution for further studies, and only the cervical vertebrae

were macerated. The synsacrum and pygostyle were examined through X-ray images obtained in the Radiological Area of the Diagnostic Imaging Service of the Hospital Escuela de la Facultad de Ciencias Veterinarias (Universidad Nacional de La Plata). The other four specimens were frozen for transportation and then thawed at room temperature for further maceration in the laboratories of the MLP. Additionally, we incorporated information from the 1-day hatchling of *A. forsteri*, available on DigiMorph (Triche, 2005).

Osteological descriptions

Osteological terms concur with Baumel and Witmer (1993), Landolt and Zweers (1984), and Livezey and Zusi (2006). Vertebrae were grouped a priori by morphological similarities and according to regions (cervical, cervicothoracic, thoracic, synsacrum, caudal and pygostyle). Then, for each region, the vertebrae were subdivided according to morphologic similarity: cervicals were grouped following the modules suggested for *A. forsteri* by Guinard and Marchand (2010), and the rest of the regions were grouped based on the morphological similarity observed directly on the material.

Descriptions include: the *corpus vertebrae* (*corpus*) in a general aspect and in cranial, caudal, ventral, and lateral perspectives; and *arcus vertebrae* (*arcus*) in cranial, caudal, and dorsal views. The order follows the position in the spine from cranial to caudal ends, indicating the element of the spine with Arabic numbers following the region letter (C: cervical, CT: cervicothoracic, T: thoracic, and Ca: free caudal).

Regionalization analysis

Vertebrae were allocated into regions according to our direct observations. Then, the morphological consistency of the cervical, cervicothoracic, and thoracic vertebrae was evaluated through a dataset constructed with the nine linear measurements proposed by Guinard et al. (2010) (Online Resource 1, Supplementary Fig. S1; Online Resource 2). A principal component analysis (PCA), using a correlation matrix, was performed using InfoStat Software 2020 version (Di Rienzo et al. 2020). The missing data (13.33%) were imputed using Euclidean distance. The total components retained were those that exceed 70% of the total accumulated variation.

Modularity analysis

Two independent datasets were used to evaluate the modularity of the cervical region of fledgling and adults. The first one was based on the outline of the articular facet of the right *processus articularis cranialis* (according to Guinard et al. 2010) of two adults (MLP-O-15192, MACN-OR-8462) and the fledgling (MLP-1014). Photographs were taken with a Panasonic Lumix LZ40 camera perpendicular to the articular facet of the right *processus articularis cranialis*. Each photo was converted to a solid black image with a white background and saved as jpg files at 300 dpi and stored in a single directory. The extraction of the silhouettes from the images, the morphogeometric analysis of the outlines of the shape, and the analysis of the data were carried out using the Momocs (Bonhomme et al. 2014) package from R (R Core Team, 2021) and carried out in RStudio (RStudio Team, 2021) software. The latest version is available at https://momx.github.io/Momocs/index.html.

The coordinates of the outlines were extracted using the import_jpg function. The resulting list was combined in a single vector to obtain a list to be analyzed. The classification category of each element was imported as a table from a txt file. The new coordinate list was classified as an Out object and inspected with the panel and stack methods. First, the outlines were smoothed with the coo_smooth function to remove the digitization noise, and then they were normalized using a sequence of the following functions: coo_center, coo_scale, coo_align_coo_slidedirection ("down"), and inspected with the stack method to corroborate the quality of the alignment and the homology of the first point of the outlines.

The quantification of the outlines was made with an elliptical Fourier analysis (EFA; Kuhl and Giardina, 1982), where the closed outlines are decomposed into a series of harmonics; each harmonic represented by four coefficients. The harmonics calibration was calculated with the calibrate_harmonicpower_efourier and calibrate_reconstruction_efourier functions to determine the appropriate number of harmonics needed to achieve 99.9% of their total power. Fourier analysis was carried out with the efourier function.

A PCA using the PCA function, followed by summary and plot_PCA functions to display the results, was performed. The number of components to retain was determined with the scree and scree_plot, and screeplot functions (the last one from the vegan package (Oksanen et al. 2020) that includes the broken stick model). To calculate and plot the variation of the shape along the axes, the PCcontrib function was used. Finally, a discriminant analysis on PC scores was performed using the LDA function, followed by plot_LDA and plot_CV functions to display the results.

The second dataset was built from linear measurements, indices, and angles, as proposed by Guinard et al. (2010) (Online Resource 1, Fig. S1; Online Resource 3). The PCA was carried out using a correlation matrix that was analyzed with InfoStat Software (Di Rienzo et al. 2020), imputing the missing data (6.56%) through Euclidean distance. The total components retained were those that exceed 70% of the total accumulated variation.

Results

Osteological descriptions

Cervical 1 (Atlas) has a ring shape (Fig. 1a–d)

Corpus The kidney-shaped *fossa condyloidea* presents a concave surface that articulates with the *condylus occipitalis* of the skull. There are two projections obliquely located in the dorsal end of this fossa. The *processus ventralis corporis* is small and keel-shaped. It is medio-ventrally located and projects caudally. The *facies articularis cranialis* is slightly convex. The *incisura fossae* is semicircular.

Arcus It is oval and mainly forms the ring of the Atlas. The *processi articulares caudales* are dorsolaterally positioned in a caudal perspective. The *processus spinosus* is absent.

Cervical 2 (Axis) (Fig. 1e–i)

Corpus It is craniocaudally elongated and its caudal half is compressed. Both *facies articularis* are located at the same level on the craniocaudal axis. The *facies articularis atlantica* is kidney-shaped, cranio-ventrally leaned, and presents a dorsal notch. The *dens axis* is cranially projected and presents a flattened dorsal surface. The *processus ventralis corporis* is highly developed and projects ventrocaudally from the caudal half of the vertebral body. The distal end of the *processus ventralis corporis* is widened. The *facies articularis caudalis* is quadrangular and saddle-shaped.

Arcus Compared to the width of the *lamina lateralis arcus*, *lamina dorsalis arcus* is very expanded. The entire arch covers approximately two thirds of the dorsal side of the vertebral body. The *processi articulare craniale* are smaller than the *processi articulares caudales*. The *processis articularis cranialis* are oval and laterally positioned. The joint surfaces are dorsoventral and faced laterally, obliquely positioned with respect to the sagittal plane and approaching each other caudally. Two small ridges are positioned ventrocaudally to the *processi articulare craniale* and slightly protrude from the *lamina lateralis arcus.* The *processi articulares caudales* have a joint surface, which is ventrally directed. Dorsally and caudally located, two semicircular bulges constitute the *tori dorsales* which have a cranially projected spine. The *processus spinosus axis* develops a widened oval distal end.

Cervicals 3–5 (Fig. 1j–x)

Corpus It is small, with the craniocaudal axis ventrally inclined, positioning both *facies articularis* in different levels. The *facies articularis cranialis* is rectangular and dorsoventrally flattened. The *foramen transversarium* is small and oval, with its major axis dorsoventrally located and progressively increasing in size in the successive vertebrae. The foramen is bounded by a thin *ansa costotransversaria* that carry two slightly marked *cristae laterale* in the three vertebrae. A *tuberculum ansae* dorsal to the crests appears only in C4 and C5. Ventrally, the *processi costale* are reduced in C3 and C4. It is thorn-shaped and caudally projected in C5. The *fovea cranioventralis* is deep and well marked, located on the cranial end (in the articulation areas with the ventral lip of the *facies articularis caudalis* of the preceding vertebra during the ventral flexion of the neck). In the caudal half, the *processus ventralis corporis* projects ventrocaudally and develops an oval and expanded distal end in C3, smaller than those of C1–2 The *processus ventralis corporis* is rounded and develops a slight caudal expansion in C4, or it is absent and two little crests cranially projected corresponding to the *processi postlaterales* are developed instead in C5. The *facies articularis caudalis* is quadrangular, saddle-shaped, and dorsoventrally elongated.

Arcus The *lamina dorsalis arcus* is laterally expanded and surpasses the lateral limits of the vertebral body. It makes the vertebra acquire a quadrangular shape in dorsal view. On the lateral limits of the *lamina lateralis arcus* there is a small and slightly marked semicircular notch located on the caudal end of C3. This notch is slightly larger in C4, and is located in the half of the *lamina dorsalis arcus* in C5. On the lateral edges of the *lamina dorsalis* there is another semicircular small and slightly marked notch in C3. The *lamina lateralis arcus*, less developed than the *lamina dorsalis arcus*, constitutes the laterals of the vertebral arch. The cranially inclined *processi articulare craniale* are semicircular in C3, oval in C4, and triangular in C5. The *processi articulares caudales* are faced ventrally. They are oval in C3, kidney-shaped in C4 and triangular in C5. Dorsal to these processes, the *tori dorsales* are strongly projected dorsolaterally. On the mediodorsal line of the *lamina dorsalis arcus*, the laterally compressed *processus spinosus* presents a rounded outline; it is slightly caudally inclined in C3 and C4, and dorsally projected in C5.

Cervical 6 (Fig. 2a–e)

Corpus It is elongated and slightly larger than C5. The *facies articularis cranialis* is rectangular, dorsoventrally compressed, and saddle-shaped. The *foramen transversarium* is large and rounded, laterally bounded by the *ansa costotransversaria*, with a dorsoventrally expanded *tuberculum processi transversi*, and a spine-shaped ventral *processi costale*, which are flattened and ventrally projected. Cranially and ventral to the *facies articularis cranialis*, the

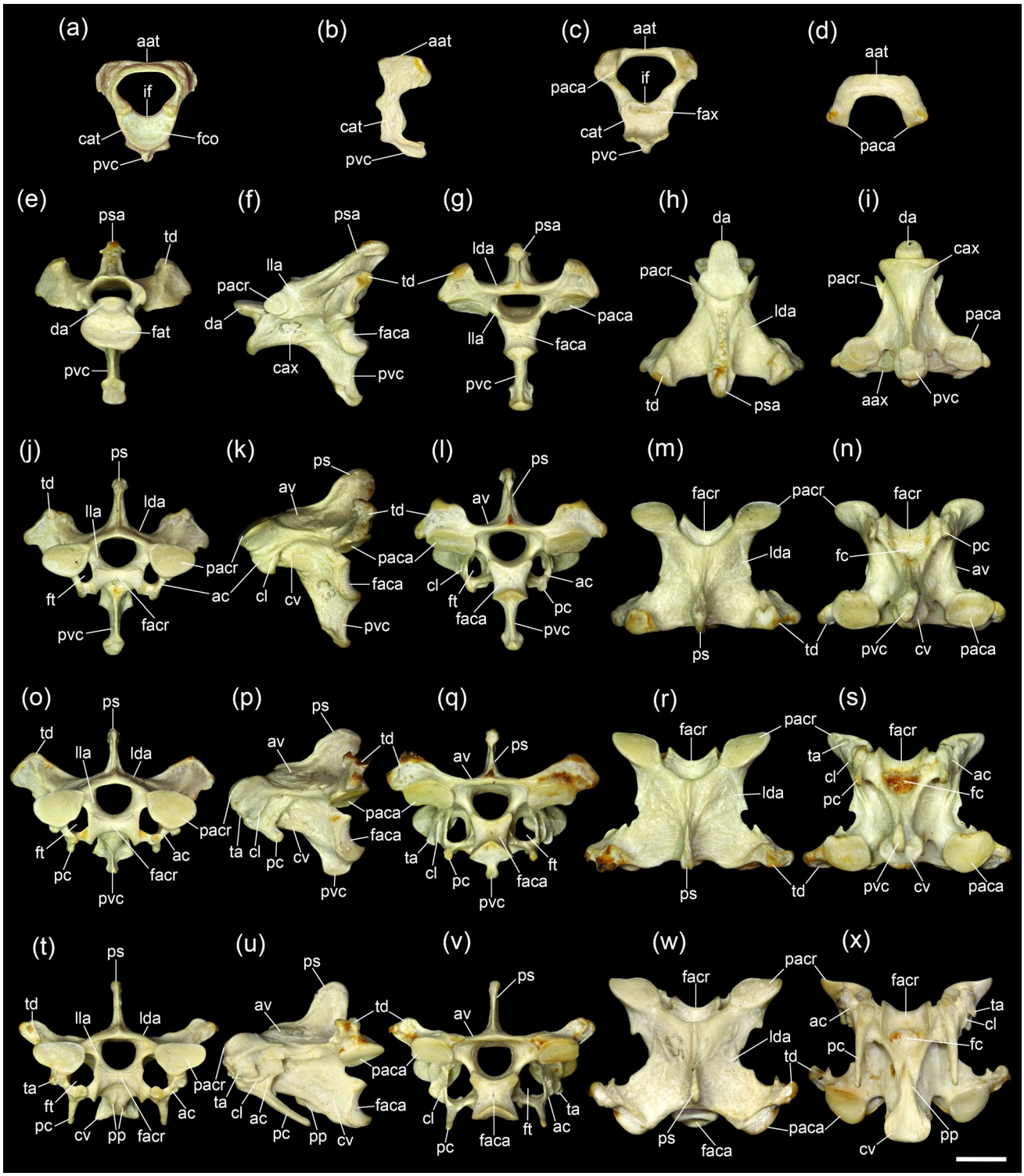

Fig. 1 Adult vertebrae MLP-O-15192. **a**–**d** C1 in **a** cranial, **b** left lateral, **c** caudal, and **d** dorsal views, **e**–**i** C2 in **e** cranial, **f** left lateral, **g** caudal, **h** dorsal, and **i** ventral views, **j**–**n** C3 in **j** cranial, **k** left lateral, **l** caudal, **m** dorsal, and **n** ventral views, **o**–**s** C4 in **o** cranial, **p** left lateral, **q** caudal, **r** dorsal, and **s** ventral views, **t**–**x** C5 in **t** cranial, **u** left lateral, **v** caudal, **w** dorsal, and **x** ventral views. aat, *arcus atlantis*; aax, *arcus axis*; ac, *ansa costotransversaria*; av, *arcus vertebrae*; cat, *corpus atlantis*; cax, *corpus axis*; cl, *cristae laterale*; cv, *corpus vertebrae*; da, *dens axis*; faca, *facies articularis caudalis*; facr, *facies articularis cranialis*; fat, *facies articularis atlantis*; fax, *facies articularis axialis*; fc, *fovea cranioventralis*; fco, *fossa condyloidea*; ft, *foramen transversarium*; if, *incisura fossae*; lda, *lamina dorsalis arcus*; lla, *lamina lateralis arcus*; paca, *processus articularis caudalis*; pacr, *processus articularis cranialis*; pc, *processus* costalis; pp, *processus postlateralis*; ps, *processus spinosus*; psa, *processus spinosus axis*; pvc, *processus ventralis corporis*; ta, *tuberculum ansae*; td, *torus dorsalis*. Scale bar 10 mm

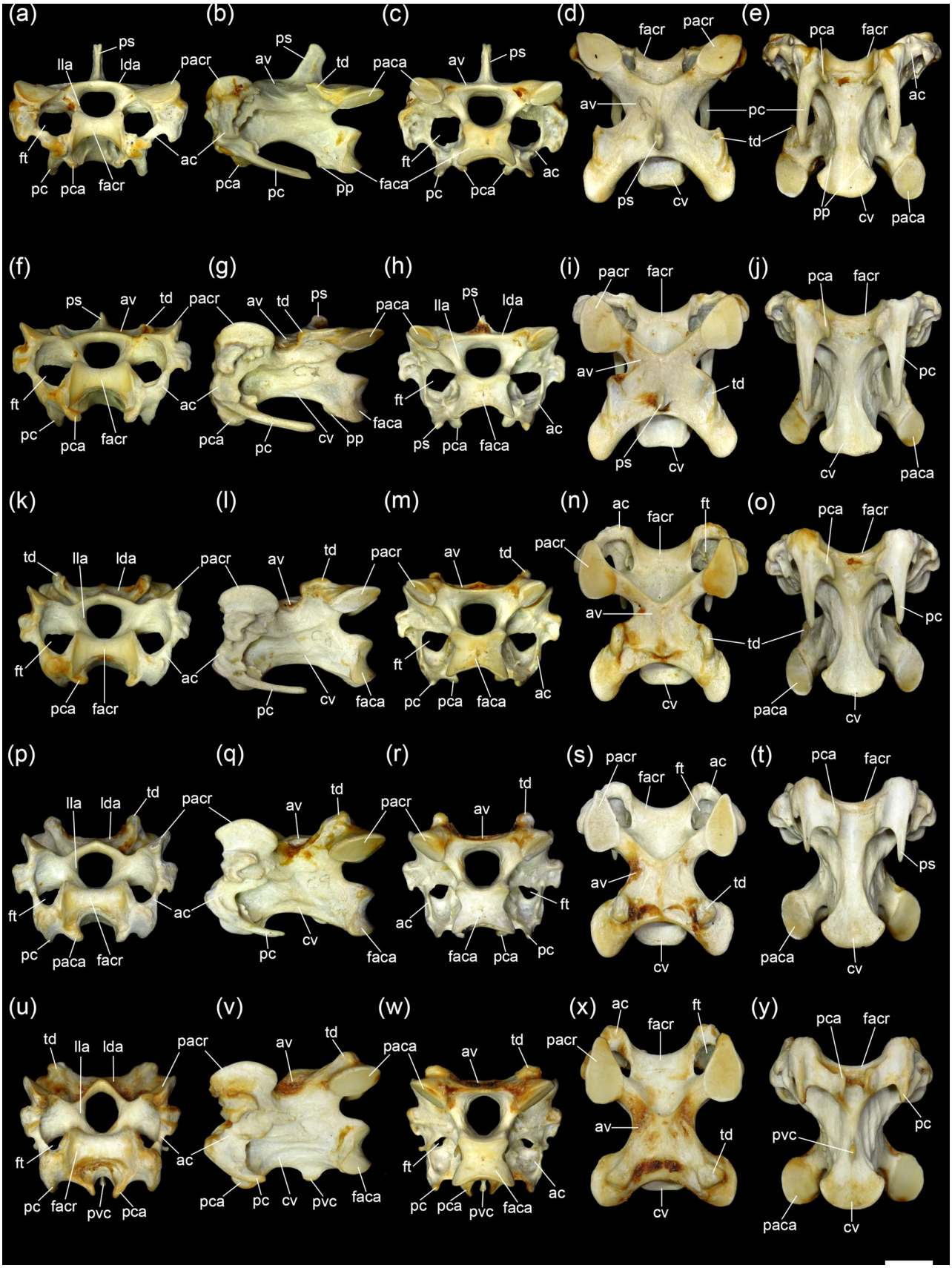
(a)
ps
lla
lda
pacr
ft
ac
pc
pca
facr
(b)
ps
av
td
pca
pc
pp
(c)
paca
av
ps
ft
faca
pc
pca
ac
(d)
facr
pacr
av
pc
td
ps
cv
(e)
pca
facr
ac
pp
cv
paca
(f)
ps
av
td
pacr
ft
ac
pc
pca
facr
(g)
av
td
ps
pca
pc
cv
pp
faca
(h)
paca
lla
ps
lda
ft
ps
pca
faca
ac
(i)
pacr
facr
av
td
ps
cv
(j)
pca
facr
pc
cv
paca
(k)
td
lla
lda
pacr
ft
ac
pca
facr
(l)
av
td
pacr
pc
cv
faca
(m)
pacr
av
td
ft
pc
pca
faca
ac
(n)
ac
facr
ft
pacr
av
td
cv
(o)
pca
facr
pc
paca
cv
(p)
lla
lda
td
pacr
ft
ac
pc
paca
facr
(q)
av
td
pacr
pc
cv
faca
(r)
td
pacr
av
ac
ft
faca
pca
pc
(s)
pacr
facr
ft
ac
av
td
cv
(t)
pca
facr
ps
paca
cv
(u)
td
lla
lda
pacr
ft
ac
pc
facr
pvc
pca
(v)
av
td
pca
pc
cv
pvc
faca
(w)
paca
av
td
ft
pc
pca
pvc
faca
ac
(x)
ac
ft
facr
pacr
av
td
cv
(y)
pca
facr
pc
pvc
paca
cv

◂**Fig. 2** Adult vertebrae MLP-O-15192. **a**–**e** C6 in **a** cranial, **b** left lateral, **c** caudal, **d** dorsal, and **e** ventral views, **f**–**j** C7 in **f** cranial, **g** left lateral, **h** caudal, **i** dorsal, and **j** ventral views, **k**–**o** C8 in **k** cranial, **l** left lateral, **m** caudal, **n** dorsal, and **o** ventral views, **p**–**t** C9 in **p** cranial, **q** left lateral, **r** caudal, **s** dorsal, and **t** ventral views, **u**–**y** C10 in **u** cranial, **v** left lateral, **w** caudal, **x** dorsal, and **y** ventral views. ac, *ansa costotransversaria*; av, *arcus vertebrae*; cv, *corpus vertebrae*; faca, *facies articularis caudalis*; facr, *facies articularis cranialis*; ft, *foramen transversarium*; lda, *lamina dorsalis arcus*; lla, *lamina lateralis arcus*; paca, *processus articularis caudalis*; pacr, *processus articularis cranialis*; pc, *processus costalis*; pca, *processus caroticus*; pp, *processus postlateralis*; ps, *processus spinosus*; pvc, *processus ventralis corporis*; td, *torus dorsalis.* Scale bar 10 mm

paired *processi carotici* enclose the *canalis caroticus cervicalis.* On the caudal end and extending cranially for about a third of the ventrolateral surface of the *corpus,* two small and flattened wing-like structures correspond to the *processi postlaterales.* The *facies articularis caudalis* is rectangular and saddle-shaped.

Arcus The *lamina dorsalis arcus* slightly exceeds the lateral limit of the *corpus* and carries a tuberculum on its caudal end. The oval *processi articulare craniale* face medially and are cranio-ventrally inclined, although the caudal most part of these processes are dorsally and barely medially faced. The oval *processi articulares caudales* face ventrolaterally, and are smaller than the *processi articulare craniale*. Dorsally, and caudally located on the *lamina dorsalis arcus*, the *tori dorsales* are distinctly flattened, tip-shaped, and cranially projected. The *processus spinosus* is thinner than those of the preceding vertebrae, with a quadrangular outline, and slightly caudally inclined. Two weak crests project from the *tori dorsales* to the *processus spinosus.*

Cervicals 7–9 (Fig. 2f–t)

Corpus It is elongated with its craniocaudal axis aligned to the spine. The *facies articularis cranialis* is trapezoidal, dorsoventrally compressed, saddle-shaped, and slightly larger than that of C6. The *foramen transversarium* is large and rounded. Laterally, the *ansa costotransversaria* has a strong dorsoventrally expanded *tuberculum processus transversi* that projects laterally beyond the limit of the *processus articularis cranialis.* Ventrally, two *cristae laterale* are developed. On the ventral side of the *ansa costotransversaria*, the *processi costale* are flattened, spine-shaped, and ventrocaudally projected, decreasing caudally in length. The *processi carotici* are similar to those of C6. On the caudal end, the *processi postlaterales* project cranially on a third of the ventrolateral surface of the *corpus* in C7, whereas they are slightly developed in C8, and absent in C9. In all these vertebrae, the *facies articularis caudalis* is quadrangular, saddle-shaped, and similar in size to that of C6.

Arcus The *lamina dorsalis arcus* slightly surpasses laterally the *corpus*; a longitudinal crest runs along the *lamina lateralis arcus* in C7 and C8; these crests are absent in C9. The *processi articulare craniale* are drop-shaped with the sharpest end pointing cranially and the articular surface slightly inclined toward the midline. The *processi articulares caudales* are oval and smaller than the *processi articulare craniale*; and the joint surface is ventrolaterally positioned. The *tori dorsales* are located on the caudal half of the *lamina dorsalis arcus* and cranial to the *processi articulares caudales*. The *tori dorsales* are flattened and tip-shaped, cranially projected in C7, oval and craniocaudally extended in C8, oval and midline-located on of the *processi articulare caudali*, and dorsally projected in C9. The *processus spinosus* is significantly smaller than that of the preceding vertebrae in C7, extremely reduced in C8, and absent in C9. Two weak crests project from the *tori dorsales* to the *processus spinosus.*

Cervicals 10–13 (Figs. 2u–y, 3a–o)

Corpus It is elongated with a horizontal and slightly inclined craniocaudalin C12. The *facies articularis cranialis* is trapezoidal and saddle-shaped, dorsoventrally compressed, and more laterally expanded than the previous ones. The *foramina transversaria* is oval and their major axis is craniocaudally oriented. These foramina are larger in C12–13. In C10–12 the *tuberculi processi transversi* are dorsoventrally expanded and do not surpass the lateral limits of the *processi articularis craniale*. In C11, however, they slightly surpass it. Two *cristae laterale* (the dorsal is stronger), are developed caudoventral to these tubercles. The *processi costale* are spine-shaped and flattened. In C10, they project caudally with a length equivalent to half the length of the previous vertebra. In C11, the *processi costale* project twice the length of C11. In C12, they are short, rounded and robust; and in C13 they are blunt and weakly developed. Only in C10, the *processi carotici* delimit a small *canalis caroticus cervicalis.* The *processus ventralis corporis* is developed from these vertebrae. It is smaller and rounded in C10; rounded, laterally compressed, and cranially inclined in C11; quadrangular and cranially inclined in C12; and smaller and ventrally projected in C13. The *processus ventralis corporis* covers two thirds of the total length of the vertebral body in C11 and C12, but only a third in C10 and C13. The *fovea cranioventralis* appears from the C11 where it is barely marked. It is also barely marked in C12, and well developed in C13. The *facies articularis caudalis* is saddle-shaped and similar in size in all the vertebrae, although in C13 it is slightly larger than in the previous ones.

Arcus The *lamina dorsalis arcus* extends laterally as much as the *corpus.* Only in C10, a weak longitudinal ridge is on

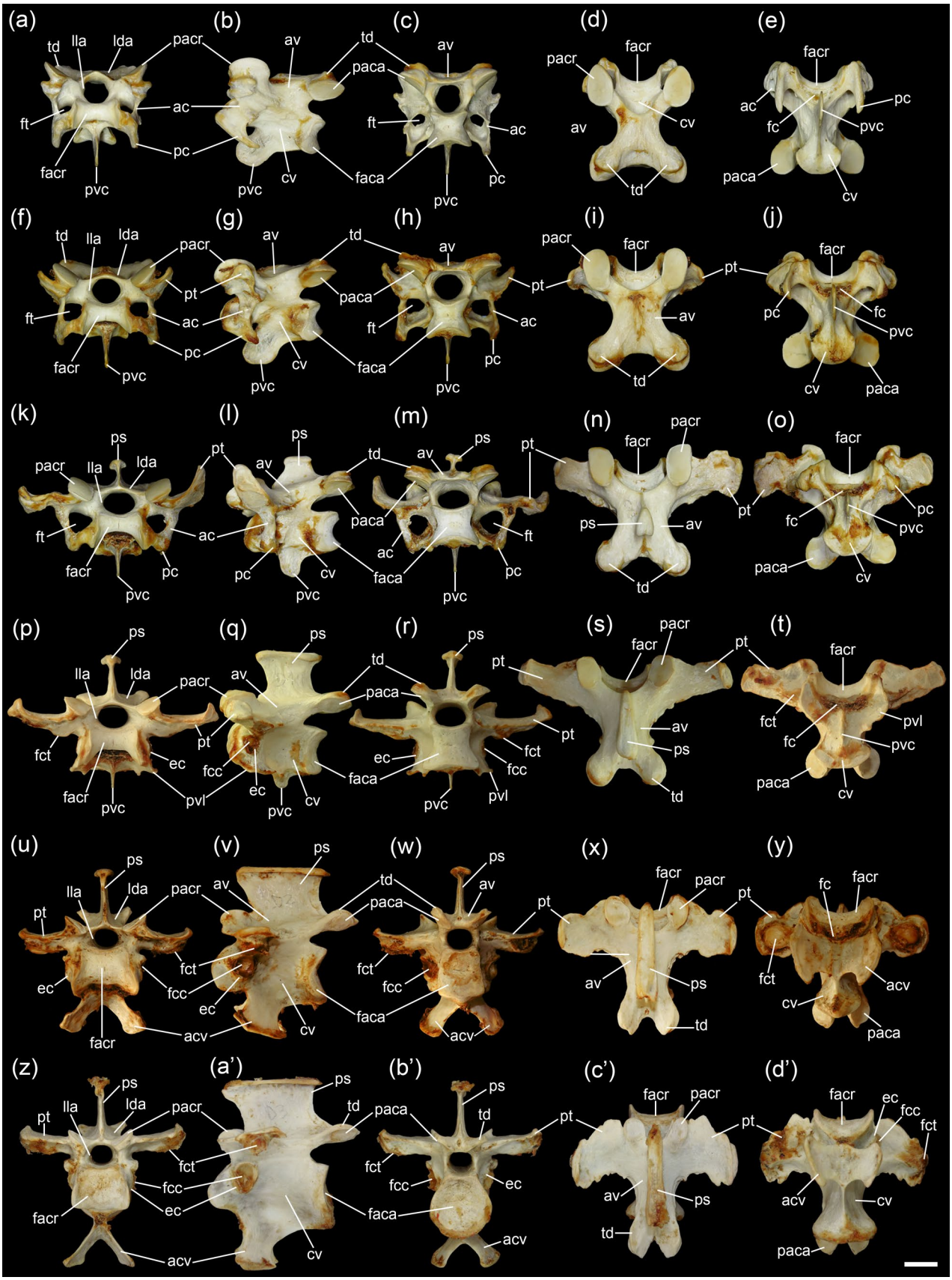
(a)
td
lla
lda
pacr
ft
ac
pc
facr
pvc
(b)
av
pvc
cv
(c)
td
av
paca
ft
ac
faca
pc
pvc
(d)
facr
pacr
av
cv
td
(e)
facr
ac
pc
fc
pvc
paca
cv
(f)
td
lla
lda
pacr
pt
ft
ac
pc
facr
pvc
(g)
av
td
paca
pvc
cv
faca
(h)
av
td
pt
paca
ft
ac
pc
faca
pvc
(i)
pacr
facr
pt
av
td
(j)
facr
pc
fc
pvc
cv
paca
(k)
ps
pacr
lla
lda
ft
ac
facr
pc
pvc
(l)
pt
ps
av
td
paca
pc
cv
pvc
(m)
ps
av
td
pt
paca
ac
ft
faca
pc
pvc
(n)
facr
pacr
ps
av
pt
td
(o)
facr
pc
fc
pvc
paca
cv
(p)
ps
lla
lda
pacr
fct
pt
ec
facr
pvc
fcc
pvl
(q)
ps
av
td
paca
ec
pvc
cv
(r)
ps
pt
td
paca
fct
ec
fcc
faca
pvc
pvl
(s)
pacr
facr
pt
av
ps
td
(t)
facr
fct
pvl
fc
pvc
paca
cv
(u)
ps
lla
lda
pacr
pt
fct
ec
fcc
facr
acv
(v)
ps
av
ec
cv
(w)
ps
td
av
paca
pt
fct
fcc
faca
acv
(x)
facr
pacr
pt
av
ps
td
(y)
fc
facr
fct
acv
cv
paca
(z)
ps
pt
lla
lda
pacr
fct
fcc
ec
facr
acv
(a')
ps
td
cv
(b')
ps
paca
td
fct
fcc
ec
faca
acv
(c')
facr
pacr
pt
av
ps
td
(d')
facr
ec
fcc
fct
acv
cv
paca

◂**Fig. 3** Adult vertebrae MLP-O-15192. **a**–**e** C11 in **a** cranial, **b** left lateral, **c** caudal, **d** dorsal, and **e** ventral views, **f**–**j** C12 in **f** cranial, **g** left lateral, **h** caudal, **i** dorsal, and **j** ventral views, **k**–**o** C13 in **k** cranial, **l** left lateral, **m** caudal, **n** dorsal, and **o** ventral views, **p**–**t** CT1 in **p** cranial, **q** left lateral, **r** caudal, **s** dorsal, and **t** ventral views, **u**–**y** CT2 in **u** cranial, **v** left lateral, **w** caudal, **x** dorsal, and **y** ventral views, **z**–**d′** T1 in **z** cranial, **a′** left lateral, **b′** caudal, **c′** dorsal, and **d′** ventral views. ac, *ansa costotransversaria*; acv, *alae cristae ventralis*; av, *arcus vertebrae*; cv, *corpus vertebrae*; ec, *eminentia costolateralis*; faca, *facies articularis caudalis*; facr, *facies articularis cranialis*; fc, *fovea cranioventralis*; fcc, *fovea costalis capituli*; fct, *fovea costalis tuberculi*; lda, *lamina dorsalis arcus*; lla, *lamina lateralis arcus*; paca, *processus articularis caudalis*; pacr, *processus articularis cranialis*; pc, *processus costalis*; ps, *processus spinosus*; pt, *processus transversus*; pvc, *processus ventralis corporis*; pvl, *processus ventrolateralis*; td, *torus dorsalis.* Scale bar 10 mm

the *lamina lateralis arcus*. The *processi articulare craniale* are drop-shaped in C10, while they are oval in the rest of the vertebrae. In a dorsal perspective, the joint surface of these processes is medially leaning in C10 and C11, and inclined toward the midline and cranially curved in C12 and C13. The *processi articulares caudales* are similar in size to the *processi articulare craniale* and their joint surface are lateroventrally leaning in C10 and C11, while in C12 and C13 they are smaller than the *processi articulare craniale*, and their joint surface are rounded and concave. The *tori dorsales* present a variable location. On C10 they are located on the medial edge of the dorsal side of the *processi articulares caudales* and caudo-laterally projected. On C11, they are expanded on the dorsal side of the *processi articulares caudales*, and extended from the caudal end to the midline. On C12, they are rounded and flattened, and expand from the caudal end to the lateral limit of these processes. On C13 they are rounded and expand over the entire dorsal surface of the *processi articulares caudales*. The *processus spinosus* is absent in C10 and C11, barely developed in C12, and well developed in C13. In the later, the *processus spinosus* is compressed and presents a heart-shaped dorsal expansion that occupies two thirds of the total length of the *lamina dorsalis arcus*. Two weak crests extend from the cranial end of the *tori dorsales* to the midline of the *arcus*. In C13, the *area ligamentum elasticum* is represented by a depression located in the midline, caudal to the *processus spinosus* and the caudal edge of the *lamina dorsalis arcus*.

Cervicothoracic 1 (Fig. 3p–t)

Corpus Rectangular and similar in size to C13. Its craniocaudal axis is aligned with the spine (not inclined). The *facies articularis cranialis* is trapezoidal, laterally elongated and saddle-shaped, larger than that of C13. Ventrally, the *fovea cranioventralis* is cranial to the small and rounded *processus ventralis corporis* that is ventrally projected. The *processus ventrolateralis* extends ventrolaterally from the lateral end of the *facies articularis cranialis* to the midline of the body. The *facies articularis caudalis* is trapezoidal and saddle-shaped, with the major axis dorsoventrally positioned. At the latero-cranial end of the vertebral body, the barely developed *eminentia costolateralis* presents a rounded *fovea costalis capituli.*

Arcus The *lamina dorsalis arcus* and the *lamina lateralis arcus* are well developed, but they do not surpass the limit of the *corpus.* The *processi articulare craniale* are oval and their main axis are craniocaudally positioned. The joint surfaces of these processes are slightly convex and inclined with the minor axis converging in the midline. The base of the *processi transversi* extends from the cranial end of the *processi articulare craniale* to the center of the vertebra. These processes spread latero-cranially, decreasing in width and bending dorsally toward the ends. The *fovea costalis tuberculi* is barely developed. The *processi articulares caudales* and *craniale* are similar in size; their joint surfaces are rounded and slightly concave. The quadrangular and laterally compressed *processus spinosus* is almost entirely covering the *lamina dorsalis arcus.* It develops a dorsal, flattened and drop-shaped expansion which is cranially oriented. Caudally, a depressed area with a triangular shape corresponds to the *area ligamentum elasticum.* The *tori dorsales* are rounded and barely developed on the dorsal surface.

Cervicothoracic 2 (Fig. 3u–y)

Corpus It is laterally compressed. The *facies articularis cranialis* is trapezoidal and saddle-shaped, with the dorsoventral axis more developed than in CT1. The *fovea cranioventralis* is slightly developed. Caudal to this fovea are the compressed and ventrolateral directed *alae cristae ventralis.* The *facies articularis caudalis* is concave and rectangular, and its major axis is dorsoventrally positioned. The *eminentia costolaterales* are slightly more developed than those of the preceding vertebra, and bear the rounded *fovea costalis capituli.*

Arcus The *processi articulare craniale* and the *processi articulares caudales* are oval and smaller than those of the preceding vertebrae. The *processi transversi* are quadrangular, wider but less laterally expanded than in CT1. Ventrally, the *fovea costalis tuberculi* is represented by a rounded protuberance. The *processus spinosus* is quadrangular and occupies the whole dorsal surface of the *lamina dorsalis arcus*.

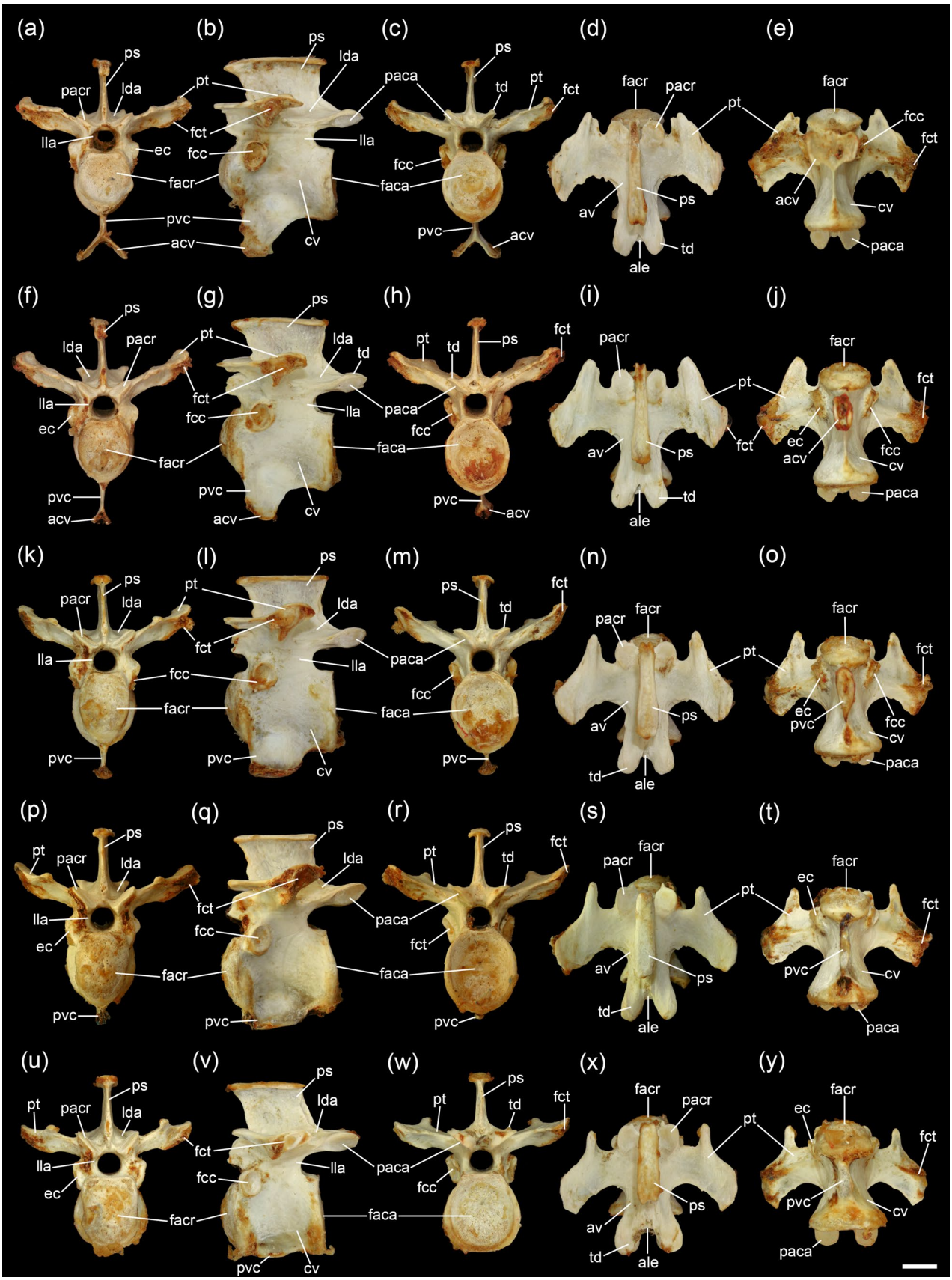
(a)
ps
pacr
lda
lla
ec
fct
facr
pvc
acv
(b)
ps
lda
pt
fct
fcc
lla
cv
(c)
ps
paca
td
pt
fct
fcc
faca
pvc
acv
(d)
facr
pacr
pt
av
ps
td
ale
(e)
facr
fcc
fct
acv
cv
paca
(f)
ps
lda
pacr
lla
ec
facr
pvc
acv
(g)
ps
pt
lda
td
fct
lla
fcc
faca
pvc
acv
cv
(h)
pt
td
ps
fct
paca
fcc
faca
pvc
acv
(i)
pacr
pt
av
ps
fct
td
ale
(j)
facr
fct
ec
acv
fcc
cv
paca
(k)
ps
pacr
lda
lla
pvc
(l)
pt
ps
lda
fct
lla
fcc
facr
pvc
cv
(m)
ps
td
fct
paca
fcc
faca
pvc
(n)
pacr
facr
pt
av
ps
td
ale
(o)
facr
fct
ec
pvc
fcc
cv
paca
(p)
pt
ps
pacr
lda
lla
ec
facr
pvc
(q)
ps
lda
fct
fcc
paca
facr
faca
pvc
(r)
ps
pt
td
fct
paca
fct
faca
pvc
(s)
facr
pacr
pt
av
ps
td
ale
(t)
facr
ec
pt
fct
pvc
cv
paca
(u)
pt
ps
pacr
lda
lla
ec
facr
(v)
ps
lda
fct
fcc
lla
facr
faca
pvc
cv
(w)
ps
pt
td
fct
paca
fcc
(x)
facr
pacr
pt
av
ps
td
ale
(y)
facr
ec
fct
pvc
cv
paca

◂**Fig. 4** Adult vertebrae MLP-O-15192. **a**–**e** T2 in **a** cranial, **b** left lateral, **c** caudal, **d** dorsal, and **e** ventral views, **f**–**j** T3 in **f** cranial, **g** left lateral, **h** caudal, **i** dorsal, and **j** ventral views, **k**–**o** T4 in **k** cranial, **l** left lateral, **m** caudal, **n** dorsal, and **o** ventral views, **p**–**t** T5 in **p** cranial, **q** left lateral, **r** caudal, **s** dorsal, and **t** ventral views, **u**–**y** T6 in **u** cranial, **v** left lateral, **w** caudal, **x** dorsal, and **y** ventral views. acv, *alae cristae ventralis*; ale, *area ligamentum elasticum*; av, *arcus vertebrae*; cv, *corpus vertebrae*; ec, *eminentia costolateralis*; faca, *facies articularis caudalis*; facr, *facies articularis cranialis*; fcc, *fovea costalis capituli*; fct, *fovea costalis tuberculi*; lda, *lamina dorsalis arcus*; lla, *lamina lateralis arcus*; paca, *processus articularis caudalis*; pacr, *processus articularis cranialis*; ps, *processus spinosus*; pt, *processus transversus*; pvc, *processus ventralis corporis*; td, *torus dorsalis.* Scale bar 10 mm

Thoracics 1–3 (Figs. 3z–d′, 4a–j)

Corpus It is laterally compressed. The *facies articularis cranialis* is saddle-shaped in T1, and rounded and concave in T2–3. In ventral view, the *processus ventralis corporis* bears a pair of ventrolaterally projected *alae cristae ventrales* that decrease in size from T1 to T3. The *alae cristae ventrales* originate on the proximal end in T1, in the center of the process in T2, and on the distal end in T3. The *facies articularis caudalis* is rounded and concave. The *eminentia costolaterales*, on the latero-cranial end of the body, bears a concave and rounded *fovea costalis capituli.*

Arcus The *lamina dorsalis arcus* and the *lamina lateralis arcus* do not exceed the lateral limits of the *corpus.* The *processi articulare craniale* are rounded and the joint surface is medially inclined in a dorsal perspective. The *processi transversi* are laterocaudally directed with the *fovea articularis tuberculi* developed on their ventral surface. In T3, the *aponeurosis ossificans* projects cranially on the cranial margin of the *processi transversi*. The *processi articulares caudales* are rounded and equal in size to the *processi articulare craniale.* Dorsally, the slightly developed and elongated *tori dorsales* occupy the whole lateral margin of the *processi articulares caudales* in T1–2, and are slightly developed in T3. The well-developed *processus spinosus* is laterally compressed and covers all the extension of the vertebral arch. This process acquires a quadrangular shape, with a dorsoventrally flattened expansion at its dorsal end.

Thoracics 4–6 (Fig. 4k–y)

Corpus It is laterally compressed. The oval *facies articularis cranialis* presents a convex joint surface. The *processus ventralis corporis* occupies approximately two thirds of the length of the vertebral body in the three vertebrae, and its size progressively decreases from T4 to T6. This process is laterally compressed and, unlike the previous vertebra, the *alae cristae ventralis* are absent. The *facies articularis caudalis* are rounded and concave. Laterocranially, the *eminentia costolateralis* bears the concave and rounded *fovea costalis capituli*.

Arcus The *lamina dorsalis arcus* and the *lamina lateralis arcus* do not exceed the lateral limits of the body. The *processi articulare craniale* are oval and the joint surface is medially inclined in a dorsal perspective. Unlike in the previous vertebrae, the *processi transversi* have a rectangular outline and are laterocaudally directed. On the cranial edge these processes present a cranial projection corresponding to the *aponeurosis ossificans* that are thinner than those of the previous vertebra. Ventrally, on the distal end of the *processus transversus*, the *fovea articularis tuberculi* is developed. The *processi articulares caudales* are rounded and their joint surfaces are laterally inclined. Both the *processi articulare craniale* and *caudale* are equal in size. Dorsally, on these processes, the *tori dorsales* develop an elongated shape. On the midline of the *lamina dorsalis arcus*, the *processus spinosus* is strongly developed, covering all the extension of the vertebral arch. It is quadrangular, laterally compressed, and presents a dorsoventrally flattened expansion at its dorsal end.

The specimen MLP-478 presents an extra thoracic vertebra (Fig. 5a, b) morphologically similar to T6, but distinguishable from it by the absence of the *processus ventralis corporis.* Furthermore, the *processi transversi* develop a caudal projection dorsally curved which contacts with the ventral side of the *ala preacetabularis ilii* of the pelvic girdle.

Synsacrum

It consists of 13 ankylosed vertebrae (Fig. 5c–h). The *corpus synsacri* is compressed at the cranial half and cylindrical at the caudal half, decreasing caudally in size. The *facies articularis cranialis* is rounded and convex. The *sulcus ventralis corporis* is absent or slightly marked, and the *facies articularis caudalis* is rounded and flattened. Each vertebra is distinguished by the opening on both sides of a rounded and small *foramina intervertebralia*. Dorsally, the *crista spinosa synsacri* extends from the cranial end of the first vertebra to the cranial end of the last synsacral one, and corresponds to the ankylosis of all the *processi spinosi*. The *crista spinosa synsacri* is compressed, dorsally thickened and progressively lower toward the caudal end. Only in some specimens, an oval foramen opens between the *processus spinosus* of the first and second vertebra. The synsacrum is divided into the 1: thoracal (TS), 2: thoracolumbar (TLS), 3: lumbar (LS), 4: sacral (SS), and 5: caudal segments (CS).

1-Thoracal segment It comprises a single vertebra corresponding to the last thoracic fused to the *synsacrum* during the ontogeny. The *corpus* is compressed and the *facies*

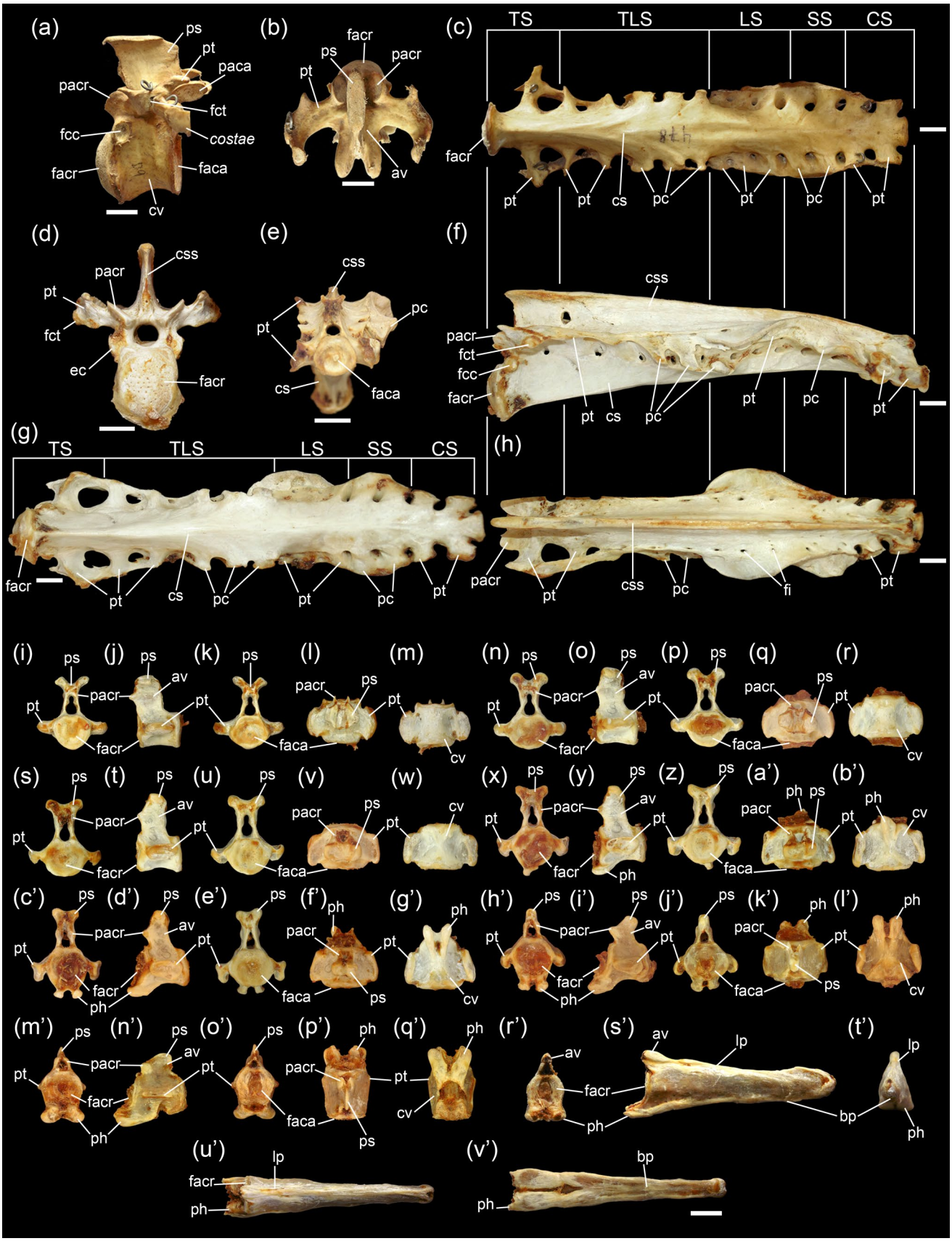
(a)
ps
pt
paca
pacr
fct
fcc
costae
facr
faca
cv
(b)
facr
ps
pacr
pt
av
(c)
TS
TLS
LS
SS
CS
facr
pt
pt
cs
pc
pt
pc
pt
(d)
css
pacr
pt
fct
ec
facr
(e)
css
pt
pc
cs
faca
(f)
css
pacr
fct
fcc
facr
pt
cs
pc
pt
pc
pt
(g)
TS
TLS
LS
SS
CS
facr
pt
cs
pc
pt
pc
pt
(h)
pacr
pt
css
pc
fi
pt
(i)
(j)
(k)
(l)
(m)
(n)
(o)
(p)
(q)
(r)
(s)
(t)
(u)
(v)
(w)
(x)
(y)
(z)
(a')
(b')
(c')
(d')
(e')
(f')
(g')
(h')
(i')
(j')
(k')
(l')
(m')
(n')
(o')
(p')
(q')
(r')
(s')
(t')
(u')
(v')
ps
av
pacr
pt
facr
faca
cv
ph
lp
bp

◂**Fig. 5** Adult vertebrae MLP-478. **a–b** T7 in **a** left lateral, and **b** dorsal views, **c** synsacrum, ventral view. Adult vertebrae MLP-O-15192. **d–h** Synsacrum in **d** cranial, **e** caudal, **f** left lateral, **g** ventral, and **h** dorsal views, **i–m** Ca1 in **i** cranial, **j** left lateral, **k** caudal, **l** dorsal, and **m** ventral views, **n–r** Ca2 in **n** cranial, **o** left lateral, **p** caudal, **q** dorsal, and **r** ventral views, **s–w** Ca3 in **s** cranial, **t** left lateral, **u** caudal, **v** dorsal, and **w** ventral views, **x–b′** Ca4 in **x** cranial, **y** left lateral, **z** caudal, **a′** dorsal, and **b′** ventral views, **c′–g′** Ca5 in **c′** cranial, **d′** left lateral, **e′** caudal, **f′** dorsal, and **g′** ventral views, **h′–l′** Ca6 in **h′** cranial, **i′** left lateral, **j′** caudal, **k′** dorsal, and **l′** ventral views, **m′–q′** Ca7 in **m′** cranial, **n′** left lateral, **o′** caudal, **p′** dorsal, and **q′** ventral views, **r′–v′** pygostyle in **r′** cranial, **s′** left lateral, **t′** caudal, **u′** dorsal, and **v′** ventral views. Synsacral segments: CS, caudal segment; LS, lumbar segment; SS, sacral segment; TLS, thoracolumbar segment; TS, thoracal segment. av, *arcus vertebrae*; bp, *basis pygostyli*; cs, *corpus synsacri*; css, *crista spinose synsacri*; cv, *corpus vertebrae*; ec, *eminentia costolaterales*; faca, *facies articularis caudalis*; facr, *facies articularis cranialis*; fcc, *fovea costalis capituli*; fct, *fovea costalis tuberculi*; fi, *foramen intertransversarium*; lp, *lamina pygostyli*; paca, *processus articularis caudalis*; pacr, *processus articularis cranialis*; pc, *processus costalis*; ph, *processus haemalis*; ps, *processus spinosus*; pt, *processus transversus.* Scale bar 10 mm

articularis cranialis is typically convex. Dorsally, the *eminentia costolaterales* are rounded. The *arcus* presents a similar configuration to that of T6, but the distal end of the *processi transversi* are dorsally curved and contact with the ventral side of the *ala preacetabularis illi*. Distally, the rounded *fovea articularis tuberculi* is developed. This vertebra is completely different in the specimen MLP-478, where the characters described above cannot be recognized and, instead, a vertebra similar to the first thoracolumbar is developed.

2-Thoracolumbar segment It includes five vertebrae, from which the first two are characterized by a compressed body and a well-developed *processi transversi* (which is longer in the first vertebra). Each process has cranial and caudal extensions contacting with the preceding and the following *processi transversi*, constituting a "bridge" for the contact with the ventral surface of the *ala preacetabularis ilii.* The following three vertebrae are more robust and their bodies are more cylindrical than the ones of the preceding vertebrae. The *processi transversi* are reduced and distinguishable only by the reduced *foramina intertransversaria.* The *processi costale*, turn caudally into a more ventral position. The *crista spinosa* is continuous along this segment, becoming caudally lower. It develops a dorsal thickening.

3-Lumbar segment It comprises three vertebrae characterized by a cylindrical and robust *corpus* without *processi costale.* The *processi transversi* present a lateral and curved expansion. The *foramina intervertebralia* has the same size as the foramina in the thoracolumbar segment. The *crista spinosa* decrease caudally in height.

4-Sacral segment It comprises two vertebrae from which the first one has the same lateral extension as the thoracal segment. The *corpus vertebrae* are depressed and wide. The *processi transversi* are short and small, and the highly reduced *foramina intertransversaria* bear large and rectangular *processi costale* which are laterally projected. The *foramina intervertebralia* are larger than those of the preceding segments. The *crista spinosa* decrease caudally.

5-Caudal segment It comprises two vertebrae that present the typical morphology of the caudal vertebrae (see below). The *corpus* are cylindrical, the *processi transversi* are rectangular and laterocaudally expanded. The *crista spinosa* has a bifid end on the last vertebra. The *facies articularis caudalis* is rounded and flattened.

Caudals 1–7 (Fig. 5i–q′)

Corpus It is cylindrical and both, the *facies articularis cranialis* and the *facies articularis caudalis*, are flat. The first three vertebrae lack any structure, but the *processus haemalis* appears in Ca4. This process is simple, or bifid and short in Ca4; and bifid and cranially projected in Ca5–7, ventrally reaching the previous vertebra.

Arcus It is dorsoventrally extended with an eight-shaped *foramen vertebrale*. The *processus spinosus* is bifid in Ca1–5 and not bifid and slightly caudally inclined in Ca6–7. The *processi transversi* are rectangular and short, dorsoventrally flattened, and expand along the vertebral body.

Pygostyle

It is formed by the fusion of the last five caudal vertebrae (Fig. 5r′–v′), compressed and triangular in lateral view, and triangular in cross section, decreasing caudally in height. The *facies articularis cranialis* is rounded and concave. The vertebral bodies are fused forming the *basis pygostyli*, although each vertebra is still distinguishable. The *arcus* are fused constituting the *lamina pygostyli* and are only differentiated in the first two vertebrae. In ventral view, the *processus haemalis* converge in a single structure at the level of the third vertebrae. This process is cranially projected beyond the ventral side of the preceding vertebra.

Ontogenetic variations

Juvenile The cervical vertebrae (Fig. 6a–e) are completely ossified, except for the distal end of all the processes (*processus ventralis corporis*, *processi transversi*, and *processus spinosus*). The *processi costale*, only proximally ossified,

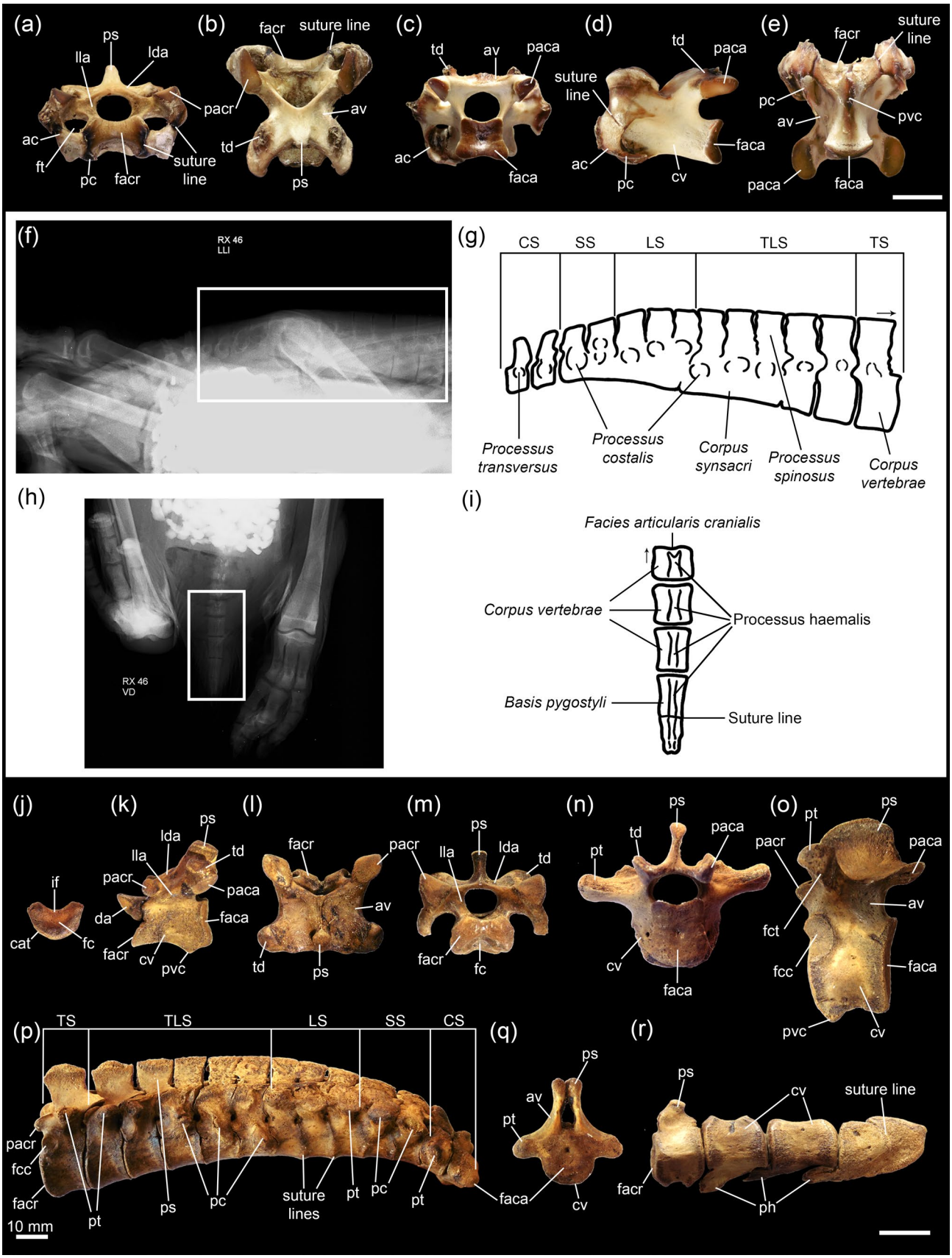
(a)
ps
lla
lda
pacr
ac
ft
pc
facr
suture line
(b)
facr
suture line
av
td
ps
(c)
td
av
paca
ac
faca
(d)
td
paca
suture line
faca
ac
pc
cv
(e)
facr
suture line
pc
av
pvc
paca
faca
(f)
RX 46
LLI
(g)
CS
SS
LS
TLS
TS
Processus transversus
Processus costalis
Corpus synsacri
Processus spinosus
Corpus vertebrae
(h)
RX 46
VD
(i)
Facies articularis cranialis
Corpus vertebrae
Processus haemalis
Basis pygostyli
Suture line
(j)
if
cat
fc
(k)
ps
lda
lla
td
pacr
paca
da
faca
facr
cv
pvc
(l)
facr
pacr
av
td
ps
(m)
ps
lla
lda
td
facr
fc
(n)
ps
td
paca
pt
cv
faca
(o)
pt
ps
pacr
paca
av
fct
fcc
faca
pvc
cv
(p)
TS
TLS
LS
SS
CS
pacr
fcc
facr
pt
ps
pc
suture lines
pt
pc
pt
faca
10 mm
(q)
ps
av
pt
faca
cv
(r)
ps
cv
suture line
facr
ph

◂**Fig. 6** Juvenile vertebrae MLP-O-15035. **a** C7, cranial view, **b** C8, dorsal view, **c** C9, caudal view, **d** C10, left lateral view, **e** C11, ventral view, **f** X-ray of the caudal zone, right lateral view, **g** scheme of the synsacrum, right lateral view, **h** X-ray of the caudal zone, ventral view, **i** scheme of the pygostyle, ventral view, **j** C1, cranial view, **k** C 2, left lateral view, **l** C6, cranial view, **m** CT1, caudal view, **n** T3, left lateral view, **o** synsacrum, left lateral view, **p** Ca3, caudal view, and **q** pygostyle, cranial view; **r** pygostyle, left lateral view. Synsacral segments: CS, caudal segment; LS, lumbar segment; SS, sacral segment; TLS, thoracolumbar segment; TS, thoracal segment. ac, *ansa costotransversaria*; av, *arcus vertebrae*; cat, *corpus atlantis*; cv, *corpus vertebrae*; da, *dens axis*; faca, *facies articularis caudalis*; facr, *facies articularis cranialis*; fc, *fovea cranioventralis*; fcc, *fovea costalis capituli*; fct, *fovea costalis tuberculi*; ft, *foramen transversarium*; if, *incisura fossae*; lda, *lamina dorsalis arcus*; lla, *lamina lateralis arcus*; paca, *processus articularis caudalis*; pacr, *processus articularis cranialis*; pc, *processus costalis*; ph, *processus haemalis*; ps, *processus spinosus*; pt, *processus transversus*; pvc, *processus ventralis corporis*; td, *torus dorsalis.* Scale bars 10 mm

are not totally fused to the rest of the vertebra; the suture line between the body and the *ansa costotransversaria* is still visible. In C10 (Fig. 6d), the *processus ventralis corporis* is absent, whereas the *processi carotici* are well developed. The elements of the synsacrum (Fig. 6f, g) are partially fused, including the bodies of the last three vertebrae of the thoracolumbar segment, the complete lumbar and sacral segments, and the first vertebra of the caudal segment. On the contrary, all the *processi spinose* are free. In the pygostyle (Fig. 6h, i), the sutures between the elements are still visible. The last two vertebrae are fused, and the rest are free.

Fledgling The *processus ventralis corporis* in C1 (Fig. 6j) is proximally ossified, whereas the *arcus atlantis* is cartilaginous. In C2 (Fig. 6k), the *dens axis* is not fused to the *corpus axis* and the distal end of the processes are free. In C3–13 (Fig. 6l, m), the *corpus* and the *arcus* are ossified, although the distal end of the *processus ventralis corporis*, *processi carotici*, *processi transversi*, and *processus spinosus* are rounded and still cartilaginous. When present, the *fovea cranioventralis* is deep and well marked. The *facies articularis cranialis* and *facies articularis caudalis* are rounded due to lack of ossification, and the *ansa costotransversaria* and the *processi costale* are absent.

In CT1–2 (Fig. 6n), the *corpus* and *arcus* are ossified. On the contrary, the *eminentia costolateralis* and the distal end of the *processus ventralis corporis*, *processi transversi* and *processus spinosus* are still cartilaginous. In T1–6 (Fig. 6o), the *corpus* and the *arcus* are completely ossified. The *processus ventralis corporis*, the distal end of the *processi transversi*, and the *processus spinosus* are rounded and still cartilaginous.

Within the synsacral vertebrae (Fig. 6p), the *corpus* of the three vertebrae of the LS are fused, with their sutures still visible. The body of the last two vertebrae of the TCS and the two vertebrae of the SS are partially fused to the LS. The *processus spinosus* is always independent. The rest of the vertebrae of the TCS, the TS, and the two vertebrae of the CS are unfused and more ovoidal in comparison with the free caudals. The *sulcus ventralis* runs along the ventral side of the LS and SS. The distal end of the *processi costale*, *processi transversus* and *processus spinosus* are still cartilaginous.

Ca1–6 (Fig. 6q) are similar to those in adults, except for the distal end of the *processi transversi*, the *processus spinosus*, and the complete *processus haemalis* that are not yet ossified. In the pygostyle (Fig. 6r), the last two vertebrae are fused and the suture is still visible. The rest of the vertebrae are still free. The *corpus* are cylindrical and each *processi spinose* are small, projected cranially, and contacting the previous vertebra.

Newborn and smallest chicks The cervical vertebrae are differentiated from the rest due to their butterfly shape (in a dorsal perspective) given by the *lamina dorsalis arcus*. Only the center of the *corpus* and the proximal end of the *processi costale* of C5–7 are ossified. Both parts of the *lamina dorsalis arcus* are unfused. The *processi articulare craniale* and the *processi articulares caudales* are the only slightly ossified processes.

The cervicothoracic vertebrae have short ribs. The *corpus* have only the center ossified, whereas all the processes are still cartilaginous. Both parts of the *arcus* are independent and the area where the *processus spinosus* will be placed remains cartilaginous. The *processi transversi* are only proximally ossified.

The thoracic vertebrae are ossified only on the center. In the *arcus*, both parts are still independent and all the processes remain cartilaginous. Only the *processi transversi* are proximally ossified.

All the synsacral vertebrae are slightly ossified and the segments are not differentiated. Each vertebral body is free and cylindrical. The *arcus* are poorly ossified.

The caudal vertebrae are poorly ossified and all the structures are very small and barely developed. The elements of the pygostyle are not differentiated from the free caudal ones.

Regionalization analysis for C–CT–T vertebrae (Online Resource 1, Supplementary Tables 1, 2)

Adults PC1 (66.1%) and PC2 (18.5%) represent the 84.6% of the explained variation (Online Resource 1, Fig. S2). The PC1 separates the cervical vertebrae which are located in the upper and lower right quadrants, from the cervicothoracics and thoracics ones, which are located in the upper and lower left quadrants. The cervicothoracics are separated

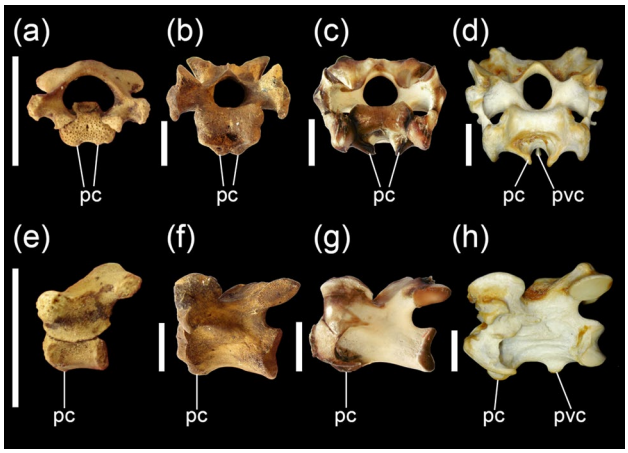

Fig. 7 Cervical 10 at different ontogenetic stages, showing the *processi carotici* (pc) and the *processus ventralis corporis* (pvc): **a** chick MLP-1010, cranial view, **b** fledgling MLP-1014, cranial view, **c** juvenile MLP-O-15035, cranial view, **d** adult MLP-O-15192, cranial view, **e** chick MLP-1010, lateral view, **f** fledgling MLP-1014, lateral view, **g** juvenile MLP-O-15035, lateral view, and **h** adult MLP-O-15192, cranial view. Scale bars 10 mm

from the thoracics by the PC2. The variables that affect the ordering of these vertebrae are K–J (the length between the cranial end and the caudal end of the *corpus*), E–F (the width between the most caudal ends of the *processi articulares caudales*), B–F (the length between the cranial end of the *processi articulare craniale*, and the caudal end of the *processi articulares caudales*), and I–J (the total length of the *arcus*) on the PC1; and L–M (the length between the *fovea cranioventralis* and the caudal end of the *corpus*), and G–H (the width of the cranial ends of the) on the PC2.

Fledgling The 84.1% of the observed variation is explained when the PC1 (54.9%) and PC2 (29.2%) are retained (Online Resource 1, Supplementary Fig. S3). Cervicals are located in the right quadrants and separated from the cervicothoracics and thoracics ordered in the left quadrants. The variables that most contributed to the ordering of the vertebrae according to regions are G–H (the width between the *tori dorsales*), E–F (the width between the most caudal ends of the *processi articulares caudales*), I–J (the total length of the *arcus*), and K–J (the length between the cranial end of the *corpus* and the caudal end of the *arcus*) on PC1; and K–N (the length between the *facies articularis cranialis* and the *facies articularis caudalis*), and L–M (the length between the *fovea cranioventralis* and the caudal end of the *corpus*) on PC2.

Modularity analyses

Elliptical Fourier analysis

Adult (MLP-O-15192) The harmonic power calibration revealed that 15 harmonics for each normalized outlines were sufficient to achieve 99.9% of the total power. The representativeness of this range was confirmed visually with the reconstructed shapes, and therefore used to do the EFA. The PCA carried out with the matrix of harmonic coefficients obtained with the EFA revealed that the cumulative proportion of the variance explained with the first three components was 92.9%. The first PC explains the shape of the articular facet placed along their horizontal axis, ranging from drop-shapes with angular ends to laterally elongated shapes. The second PC explains the roundness of the shapes. The third PC explains the lateral variations of the shapes, varying from concave to convex to straight sides.

Even though the broken stick model limited the number of PCs to three, an LDA was carried out revealing that, under the highest precision for the discrimination of the groups, the number of PC to retain was six. This value was used to carry out the discriminant analysis, which allowed the ordering of the groups. The first two LD axes captured 93.1% of the variance between groups. The first LD corresponds to the axis that clearly separates the groups that correspond to Mo2–5–6 from the groups that correspond to Mo3–4. The second LD corresponds to the axis that slightly discriminates the Mo2–4 from Mo5, and from the groups of Mo3–6. The leave-one-out cross-validation, had a classification accuracy of only 20%, classifying correctly only two out of ten elements, whereas its precision was also low (see Online Resource 1, Supplementary Figs. S4, S5, S6, S7, S8, S9, S10, S11, S12, S13, S14).

Adult (MACN-OR-8462) In this analysis, the harmonic power calibration revealed that 22 harmonics for each normalized outline were sufficient to achieve 99.9% of the total power. The results of the PCA revealed a 79.1% of the cumulative proportion of the variance explained with the first two components. The first PC captured the variation of the shape along a horizontal axis of the articular facet, meaning that it explains the width of said facets. The second PC captured the variation of the shape along the longitudinal axis of the facet, explaining the length of the articular facets, and the roundness or angularity of its ends.

The broken stick model limited the number of PCs to two, and the LDA carried out revealed that the number of PC to retain was seven. This value was used to carry out the discriminant analysis, which allowed the ordering of the groups. The first two LD axes captured 99.9% of the variance between groups. The first LD corresponds to the axis that clearly separates all the groups corresponding to

all the modules. The second LD corresponds to the axis that slightly discriminates the Mo5–3 from Mo4 to 6 groups. The leave-one-out cross-validation had a classification accuracy of only 11.1%, classifying correctly only one out of nine elements, whereas the precision was also low (see Online Resource 1, Supplementary Figs. S15, S16, S17, S18, S19, S20, S21, S22, S23, S24, S25).

Fledgling (MLP-1014) Harmonic power calibration revealed that 14 harmonics for each normalized outline were enough to achieve 99.9% of total power. The PCA using the harmonic coefficients matrix revealed a 95.7% of cumulated variance explained with the first three components. The first PC explains the variation of the shape in the upper end of the articular facets, varying from angular to rounded. The second PC explains the variability of the shape at the lower end, also varying from angular to rounded. The third PC explains the width of the articular facet, varying from rounded to oval shaped.

The broken stick model limited the number of PCs to three, and the LDA carried out revealed that the number of PC to retain was five. The discriminant analysis carried out with this value allowed the ordering of the groups. The first two LD axes captured 99.9% of the variance between groups. The first LD corresponds to the axis that clearly separates the Mo5, the Mo6 and the Mo3–4 groups. The second LD corresponds to the axis that slightly discriminates the Mo3 from the Mo4 groups. The leave-one-out cross-validation had a classification accuracy of 50%, classifying correctly five out of ten elements, whereas the precision was low (see Online Resource 1, Supplementary Figs. S26, S27, S28, S29, S30, S31, S32, S33, S34, S35, S36).

Linear measurements

The PCA based on linear measurements allowed the determination of modules according to morphological similarity (Online Resource 1, Tables 6, 7).

Adults PC1 represents the 61.2% of the total variation, and PC2 adds the 18.5%, representing the 79.7% of the accumulated explained variation (Online Resource 1, Supplementary Fig. S37). The PC1 shows the vertebrae corresponding to Mo3 (C3–5) on the left side of the graph separated from the rest which are located on the right. The PC2 separates the vertebrae of Mo4 and Mo5 (C6–9) on the lower part of the graph, from those of Mo6 (C10–13) shown on the upper part. In turn, among the former, the Mo4 (C6) can be differentiated from the others vertebrae of the Mo5. The variables with the greatest weight were I3 (development of the *ansa costotransversaria*), I4 (elongation index), L–M (the length between the *fovea cranioventralis* and the *facies articularis caudalis*), Ang (angle between *processi articulare craniale*), and K–N (the length between the *facies articularis cranialis* and the *facies articularis caudalis*) on the PC1; and K–J (the length between the cranial end of the *corpus* and the caudal end of the *arcus*), I3 (development of the *ansa costotransversaria*), B–F (the length between the cranial end of the *processi articulare craniale* and the caudal end of the *processi articulares caudales*), and I–J (the length of the *arcus*) on the PC2.

Fledgling PC1 gathers the 57.1% of the explained variation, and PC2 accumulates a 27.0% more, making a total of 84.1% of the variation (Online Resource 1, Supplementary Fig. S38). The PC1 divides the vertebrae of Mo3 (C3–5) in the lower left quadrant, from those of Mo4 (C6) and Mo5 (C7–9) in the right lower quadrant. The vertebrae of Mo6 (C11–13) are grouped on the upper right and left quadrants. The variables that affect the ordering of these vertebrae are K–N (the length between the *facies articularis cranialis* and the *facies articularis caudalis*), I3 (development of the *ansa costotransversaria*), B–F (the length between the cranial end of the *processi articulare craniale* and the caudal end of the *processi articulares caudales*), and G–H (the width between the *tori dorsales*) on the PC1; and I–J (the length of the *arcus*), I2 (development or functional part of the *facies articularis caudalis*), A–B (the width between the most cranial ends of the *processi articulare craniale*); and I3 (development of the *ansa costotransversaria*) on the PC2.

Discussion and conclusions

Remarks on spine morphology and regionalization

The comparative morphology and the morphometric analyses of the cervical, cervicothoracic, and thoracic vertebrae of *A. forsteri* allowed us to recognize the same regions previously known for other penguin species. The spine of *A. forsteri* presents 42/43 vertebrae divided as follows: 13 cervicals, 2 cervicothoracics, 6/7 thoracics, 13 vertebrae fused into a synsacrum, 7 free caudals, and 5 caudals fused into a pygostyle (counted here as a single vertebral element).

Our results are coherent with the morphological descriptions of the cervicals for penguins provided by Zusi (1962) and Baumel and Witmer (1993), and the number of elements established by Watson (1883), Stephan (1979), Guinard et al. (2010), and Guinard and Marchand (2010). Except for C1 (Atlas) and C2 (Axis), the remaining cervical vertebrae are characterized by a homogeneous morphology, which is reflected in the PCA analyses.

The characters described above vary according to their location on the spine. The *processus ventralis corporis* is projected caudally in C2–4 and cranially in C11–13. The *fovea cranioventralis* is only present in these same vertebrae.

The *processus ventralis corporis* and the *fovea cranioventralis* are absent in the middle region of the neck (C5–10), where the *processi carotici* appear delimiting the *sulcus caroticus.* The *processus spinosus* appears with a variable development and inclination in the cranialmost (C2–7) and caudalmost (C13) vertebrae, and it is reduced or absent in the vertebrae of the middle region (C8–12). The *processi articulare craniale* varies from rounded (C2–5) to teardrop-shaped (C6–10) or oval (C11–13), and it is dorsomedially (C3–6, C12–13) or dorsocranially (C7–11) positioned along the neck. The *tori dorsales* varies from blunt (C2–5) to elongated (C10–12) and are located at the caudal end of the *lamina dorsalis arcus* (on the *processi articulares caudales*), or cranially displaced in the vertebrae of the middle region (C6–9). Among living species, the axis presents a peculiarity. Although the general morphology is similar to the rest of the cervicals, a distal expansion appears on the *processus ventralis corporis*; feature also observed in the fossil penguin *Icadyptes salasi* (see Ksepka et al. 2008).

The cervicothoracic vertebrae are morphologically intermediate between the cervicals and the thoracics. The similarities with the last cervicals and the first thoracics are also reflected in the PCA analysis. Like the cervicals, the cervicothoracics are heterocoelous, with a flattened vertebral body and a well-developed *processus ventralis corporis*, *processi transversi* laterally elongated with a dorsal curvature at the distal end, and oval and large projected *processi articulare craniale* dorsocranially. Like the thoracics, the cervicothoracics are laterally compressed and present a rectangular *processus spinosus*, and *eminentia costolaterales* for the articulation of the ribs. Precisely, the presence of non-fused but short ribs that do not contact the *sternum* is the distinctive feature of these vertebrae. Beyond the similarities with the cervicals and thoracics, and from a morpho-functional perspective, the cervicothoracics could be considered as a part of the neck (see Vanden Berge 1999).

In agreement with Shufeldt (1901), we counted six opisthocoelous vertebrae in the thoracic region (see also Shufeldt 1901; Baumel and Witmer 1993). These vertebrae are characterized by a high and laterally compressed *corpus.* The first thoracic vertebra (T1) presents heterocoelous *facies articularis cranialis*, although the *facies articularis caudalis* is concave. This heterocoelous condition for the cranial end of the *corpus* of T1 has already been observed in *E. chrysocome* by Watson (1883), and in *P. papua* by Jadwiszczak (2014a). The *processus ventralis corporis* is highly developed, especially in T1–4. From T1 to 3, this process is bifid, character related to diving adaptations (Kuroda 1954). In this region, the *arcus* extends laterally beyond the vertebral body. As it was observed by Watson (1883), the *processus spinosus* is rectangular and spanning the entire arch. It is laterally compressed, and has a flattened distal expansion in all the vertebrae of this region. Caudal to this process is an angular notch (*area ligamentum elasticum*) where the interlaminar and interspinous elastic ligaments are inserted (Baumel and Witmer 1993). Unlike the *processi articulare* of the vertebrae of the previous two regions, the *processi articulare craniale* and *processi articulares caudales* of the thoracics are small and rounded; projected dorsally and ventrally, respectively. These vertebrae also have highly developed *processi transversi* that are flattened and directed backwards with the *eminentia costolateralis* on the ventral surface of the distal ends of these processes, as it was also described by Watson (1883). These vertebrae articulate with each other constituting a straight and rigid structure.

The synsacrum, formed by the fusion of 13 vertebrae in the adult, is composed by 5 segments, (Stephan, 1979). The free caudals have a distinctive morphology with respect to the other regions. These vertebrae have a cylindrical *corpus* and a triangular *arcus*. Contrarily with the observations of Watson (1883), who described a distally bifid *processus spinosus* in Ca1–4 only, the specimens here examined have this condition in Ca1–5 and a simple and distally curved distal end in Ca6–7. The *processus transversus* are rectangular and flattened as described by Watson (1883). Although the fusion of six to seven vertebrae along the ontogeny of penguins was described by Stephan (1979) and Pycraft (1898), we found only five vertebrae fused into the pygostyle of *A. forsteri.*

Remarks on individual variations

A numerical variation was observed in the thoracic region of the specimen MLP-478. As we described above, the thoracic region of *A. forsteri* is characterized by the presence of six vertebrae. However, MLP-478 has seven thoracic vertebrae. The last of these vertebrae (named here as T7, Fig. 5a, b) is morphologically indistinguishable from the rest of the thoracics. It means that the *corpus* is opisthocoelous, the *arcus* does not extend beyond the laterals of the vertebral body, the *processi articulare craniale* and *caudale* are small and rounded, the *processus spinosus* is quadrangular and compressed and covers the entire extension of the arch, and the *eminentia costolaterales* are developed. However, T7 is completely devoid of *processus ventralis corporis*, and the distal end of the *processi transversi* are dorsally curved and contact the ventral side of the *ala preacetabularis ilii*; morphology found in the thoracal segment of the synsacrum in the rest of the specimens. However, if T7 would correspond to the thoracal segment, the synsacrum of specimen MLP-478 would have only twelve fused vertebrae. This is not the case since the synsacrum of MLP-478 has the thirteen vertebrae described above (Fig. 5c), plus the additional

T7 element. Another particular condition is that the first synsacral vertebra of MLP-478 presents a morphology according to the thoracolumbar segment. We discard that T7 could correspond to the thoracal segment due to the absence of the suture lines between the synsacral segments that characterize the sub-adult.

The presence of the T7 could represent an intra-specific condition or a frequent abnormality. These numerical variations in the spine elements were already described in humans (Decker 1915; Cimen and Elden 1999) and treated numerical anomalies (Oostra et al. 2005) in goats (Simoens et al. 1983), and cranes (Family Gruidae) within wild birds (Hiraga et al. 2014). As the case reported here, these anomalies usually occur in transitional zones.

Remarks on ontogenetic variations

As expected, differences in the ossification degree of the vertebral elements between each region appear along the postnatal ontogeny. None of the spine elements in chicks are completely developed, and the *corpus* are always separated from the *arcus.* The *processi costale* of the cervical vertebrae are partially ossified, but not fused to the vertebrae in C5–7. Neither the synsacrum nor the pygostyle are formed; therefore, all the constituting vertebra are free.

The ossification is greater in fledgling specimens, in which each vertebra partially acquires the adult configuration and, therefore, they can be grouped according to regions. The cervicothoracic region is not completely defined, although the particular features of these vertebrae are already present. Although the synsacrum is not completely developed (only the lumbar segment is fused), each vertebra is perfectly distinguishable based on their oval body and general proportions (laterally wide and craniocaudally short shape). The same occurs with the pygostyle, which is still unfused, but each vertebra exhibits a distinctive shape that makes them also differentiable from the free caudals. In juveniles, the vertebrae are fully formed, and differ from adults due to the size and the presence of the suture lines between the elements. The suture lines between the elements of the synsacrum are also observed in juveniles of *Aptenodytes* and *Pygoscelis* specimens (Jadwiszczak 2014b). Only in the adult stage the whole spine is completely ossified and the sutures between the elements disappear.

Remarks on modularity

Although the outline of the articular facet of the right *processus articularis cranialis* was a useful tool for the recognition of cervical modules in other penguins (see Guinard et al. 2010), this parameter it was not as adequate as expected for their recognition in *A. forsteri*. The results of the PCA in adults and fledglings were not clear in determining the different modules. Clearer results were obtained in the LDA were the vertebrae of each module were slightly grouped. The grouping of the vertebrae into modules was more notable in adults, where Mo2 (Axis) groups vertebrae with a particular oval shape and a lateral prominence; Mo3 (C3–5) is characterized by being laterally elongated, and triangular to oval in shape; Mo4 (C6) tends to be quadrangular; Mo5 (C7–9) differs by being drop-shaped; and Mo6 (C10–13) is oval and longitudinally elongated. In the fledgling, this groups were not so clear. Although the vertebral groups corresponding to the modules showed some differentiation, this was not so marked. This can be attributed to the fact that at this stage the *processi articulare craniale* are characterized by being mostly oval in shape, and not completely ossified.

In contrast, when using linear measurements, the same modules recognized for the cervical region of other penguin species were recognized in *A. forsteri.* Mo1 (C1 or atlas) and Mo2 (C2 or axis) are composed by a single element, Mo3 includes the C3, C4, and C5, elements. Mo4, called "transitional" (Guinard et al. 2010), is represented by C6. Mo5, is represented by vertebrae C7 to C9.

It is necessary to highlight a particularity with respect to Mo6. According to previous observations made in *A. patagonicus* and *P. papua* during the postnatal ontogeny, the main identifying character of Mo6 should be the sudden appearance of the *processus ventralis corporis* accompanied by the disappearance of the *processi carotici* in C10 (Guinard et al. 2010). The C10 of the adult MLP-O-15192 (Fig. 7d, h) has a barely developed *processus ventralis corporis* accompanied by the *processi carotici.* Further comparisons were not possible due to the lack of preservation of C10 in MACN-OR-8462 and MLP-478. As this transformation occurs during growth, the *processus ventralis corporis* in C10 could be a vestige of the pre-adult stages. However, this process is not present in any of the immature specimens studied here (Fig. 7a–c, e–g). In fledgling and juveniles, the *processus ventralis corporis* is ossified in vertebrae C11 to C13. This feature is relevant in terms of neck mobility because the *M. longus colli ventralis* inserts on the *processus ventralis corporis* of the most caudal vertebrae and the *processus caroticus* of the mid-cervical region (Baumel and Witmer 1993).

Remarks on the mobility of the neck

Given that individuals of *A. forsteri* begin their aquatic life once they molt (Stonehouse 1953), several skeletal and muscular structures are not completely developed while they are kept on land and fed by their parents. The spine, and particularly the neck muscles, are a clear example of that.

As excellent swimmers, penguins require a hydrodynamic shape to optimize their underwater movements. Thanks to the variated morphology of the vertebrae along the spine,

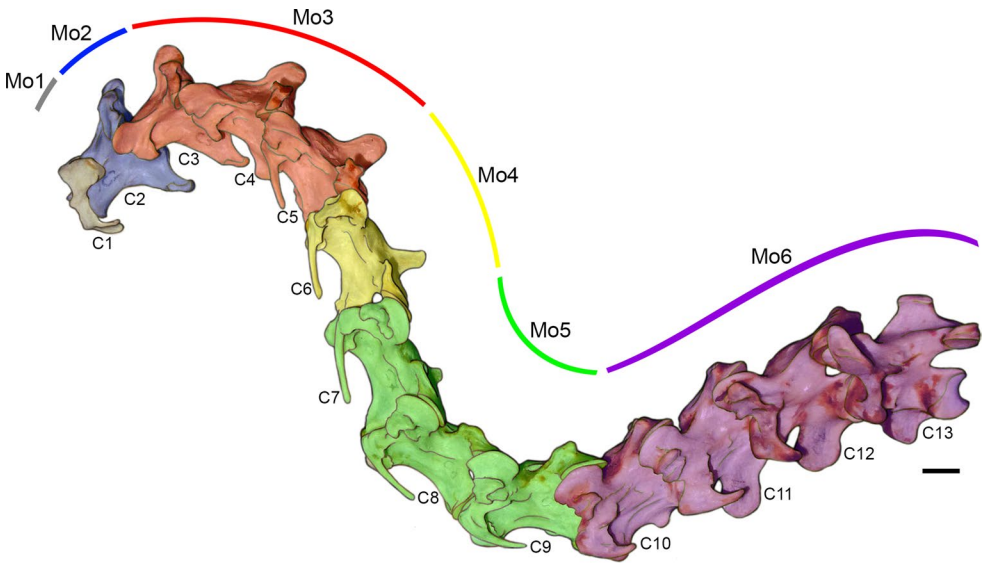

Fig. 8 Schematic draw showing the modularity in the neck of *Aptenodytes forsteri*, MLP-O-15192 left lateral view. Mo indicates the modules; C1–13 indicates the number of cervical vertebrae. Scale bar 10 mm

the neck acquires an S-shape during diving and the head is retracted against the body (Guinard et al. 2010). However, this is not possible if the ossification degree is insufficient, situation observed in the chicks here examined.

A significant change in the ossification degree and the development of the articular surfaces that participate in the spine mobility is observed in the juveniles of *A. forsteri*. Although the involved structures are not fully fused yet, the characteristic S-shape observed in penguins is already marked. Equivalent ontogenetic stages examined in other penguin species were considered unsuitable for an efficient diving (Guinard et al. 2010).

In adults with the spine completely developed, and as in other penguin species, the S-shaped is automatically generated by contacting each of the cervical vertebrae (Fig. 8). The first ventral curvature of the neck is determined by Mo1, Mo2, and Mo3; Mo4 is interpreted as transitional. The following dorsal curvature (mechanical curvature sensu Guinard et al. 2010) is represented by Mo5. The second ventral curvature is restricted to Mo6 which contacts with the cervicothoracic region. Summarizing, this modular organization in the curvatures of the neck is coincident with that proposed for other adult penguins by Guinard et al. (2010).

Supplementary Information The online version contains supplementary material available at https://doi.org/10.1007/s00300-021-02986-2.

Acknowledgements We mainly thank the Instituto Antártico Argentino (Dirección Nacional del Antártico) for supporting the field trip. Dr. Leopoldo Soibelzon and Dra. Marcela Libertelli for the collected material, and Dr. Diego Montalti and Dra. Mariana Picasso for the access to the material. To Walter Acosta for his help in taking the X-rays. María Florencia Sosa who improved the English grammar. M.A.S. thanks Jorge La Grotteria who helped with R syntax. This is a contribution of the Project N955 of the Universidad Nacional de La Plata. We thank Julian Hume, two anonymous reviewers and the editor for their helpful comments.

Author contributions MAS and CAH devised the project, delineated the main conceptual ideas and designed the study. MAS performed the dissections and relieved the data and CAH supervised the project. MAS and CAH interpreted and discussed the results, and wrote the manuscript. MAS prepared the figures.

Funding Funding information is not applicable.

Declarations

Conflict of interest The authors declare that there is no conflict of interest.

Ethical approval Use of this animal in research does not require ethical clearance. Specimens were collected in Snow Hill Island (Antarctica) immediately after natural death during the austral summer field trip of 2014 by members of the Instituto Antártico Argentino (IAA).

Informed consent Authors agreed with the content and gave explicit consent to submit.

References

Baumel JJ (1988) Functional morphology of the tail apparatus of the pigeon (*Columba livia*). Adv Anat Embryol Cell Biol 110:1–115

Baumel JJ, Witmer LM (1993) Osteologia. In: Baumel JJ, King SA, Breazile JE, Evans HE, Berge JC (eds) Handbook of avian anatomy: Nomina anatomica avium. Publications of the Nuttall Ornithological Club, Cambridge, pp 45–132

Bonhomme V, Picq S, Gaucherel C, Claude J (2014) Momocs: outline analysis using R. J Stat Softw 56:1–24. https://doi.org/10.18637/jss.v056.i13

Cherel Y, Kooyman GL (1998) Food of Emperor Penguins (*Aptenodytes forsteri*) in the western Ross Sea, Antarctica. Mar Biol 130:335–344

Cimen M, Elden H (1999) Numerical variations in human vertebral column. Okajimas Folia Anat Jpn 75:297–303
Decker HR (1915) Report of the anomalies in a subject with a supernumerary lumbar vertebra. Anat Rec 9:181–189
Di Rienzo JA, Casanoves F, Balzarini MG, Gonzalez L, Tablada M, Robledo CW (2020) InfoStat version. Centro de Transferencia InfoStat, FCA, Universidad Nacional de Córdoba. http://www.infostat.com.ar. Accessed 5 May 2020
Fürbringer M (1888) Untersuchungen zur Morphologie und Systematik der Vögel: zugleich ein Beitrag zur Anatomie der Stütz-und Bewegungsorgane. T. Van Holkema, Amsterdam
Galbusera F (2018) The spine: its evolution, function, and shape. In: Biomechanics of the spine. Academic, New York, pp 3–9
Galbusera F, Bassani T (2019) The spine: a strong, stable, and flexible structure with biomimetics potential. Biomimetics 4:60
Guinard G, Marchand D (2010) Modularity and complete natural homeoses in cervical vertebrae of extant and extinct penguins (Aves: Sphenisciformes). Evol Biol 37:210–226
Guinard G, Marchand D, Courant F, Gauthier-Clerc M, Le Bohec C (2010) Morphology, ontogenesis and mechanics of cervical vertebrae in four species of penguins (Aves: Spheniscidae). Polar Biol 33:807–822
Hiraga T, Sakamoto H, Nishikawa S, Muneuchi I, Ueda H, Inoue M, Shimura R, Uebayashi A, Yasuda N, Momose K, Masatomi H, Masatomi H (2014) Vertebral formula in red-crowned crane (*Grus japonensis*) and hooded crane (*Grus monacha*). J Vet Sci 76:503–508
Isenmann P, Jouventin P (1970) Eco-éthologie du manchot empereur (*Aptenodytes forsteri*) et comparaison avec le manchot Adélie (*Pygoscelis adeliae*) et le manchot royal (*Aptenodytes patagonica*): conséquences du problème du territoire sur l'organisation sociale à la colonie. L'oiseau R.F.O. 40:136–159
Jadwiszczak P (2014a) At the root of the early penguin neck: a study of the only two cervicodorsal spines recovered from the Eocene of Antarctica. Polar Res. https://doi.org/10.3402/polar.v33.23861
Jadwiszczak P (2014b) Synsacra of the Eocene Antarctic penguins: new data on spinal maturation and an insight into their role in the control of walking. Pol Polar Res 35:27–39
Jouventin P (1971) Comportement et structure sociale chez le manchot empereur. La Terre et la Vie 25:510–586
Klages N (1989) Food and feeding ecology of Emperor Penguins in the Eastern Weddell Sea. Polar Biol 9:385–390
Klingenberg CP (2002) Morphometrics and the role of the phenotype in studies of the evolution of developmental mechanisms. Gene 287:3–10
Ksepka DT, Clarke JA, DeVries TJ, Urbina M (2008) Osteology of *Icadyptes salasi*, a giant penguin from the Eocene of Peru. J Anat 213:131–147
Kuhl FP, Giardina CR (1982) Elliptic Fourier features of a closed contour. Comput Graph Image Process 18:236–258
Kuroda N (1954) On some osteological and anatomical characters of Japanese Alcidae (Aves). Jpn J Zool 11:311–327
Landolt R, Zweers G (1984) Anatomy of the muscle-bone apparatus of the cervical system in the mallard (*Anas platyrhynchos* L.). Neth J Zool 35:611–670
Livezey BC, Zusi RL (2006) Higher-order phylogeny of modern birds (Theropoda, Aves: Neornithes) based on comparative anatomy: I. Methods and characters. Bull Carnegie Mus Nat Hist 37:1–544
Martínez I, Christie DA, Jutglar F, Garcia EFJ (2020) Emperor Penguin (*Aptenodytes forsteri*), version 1.0. In: del Hoyo J, Elliott A, Sargatal J, Christie DA, de Juana E (eds) Birds of the world. Cornell Lab of Ornithology, Ithaca. https://doi.org/10.2173/bow.emppen1.01
Newton A (1896) A dictionary of birds. Adam and Charles Black, London
Oksanen J, Guillaume Blanchet F, Friendly M, Kindt R, Legendre P, McGlinn D, Minchin PR, O'Hara RB, Simpson GL, Solymos P, Stevens MHH, Szoecs E, Wagner H (2020) Vegan: community ecology package. R package version 2.5-7. https://CRAN.R-project.org/package=vegan. Accessed 7 October 2021
Oostra RJ, Hennekam RC, de Rooij L, Moorman AF (2005) Malformations of the axial skeleton in Museum Vrolik I: homeotic transformations and numerical anomalies. Am J Med Genet 134:268–281
Prévost J (1961) Écologie du manchot empereur *Aptenodytes forsteri* Gray. Hermann
Pycraft WP (1898) Contributions to the osteology of birds. Part I. Steganopodes. Proc Zool Soc Oxf UK 66:82–101
R Core Team (2021) R: a language and environment for statistical computing. R Foundation for Statistical Computing, Vienna. https://www.R-project.org/. Accessed 7 October 2021
RStudio Team (2021) RStudio: integrated development for R. RStudio, Inc., Boston. http://www.rstudio.com/. Accessed 7 October 2021
Shufeldt RW (1901) Osteology of the penguins. J Anat Physiol 35:390
Simoens P, Vos ND, Lauwers H, Nicaise M (1983) Numerical vertebral variations and transitional vertebrae in the goat. Anat Histol Embryol 12:97–103
Sosa MA, Acosta Hospitaleche C (2018) Ontogenetic variations of the head of *Aptenodytes forsteri* (Aves, Sphenisciformes): muscular and skull morphology. Polar Biol 41:225–235
Stephan B (1979) Vergleichende OSleologie der Pínguine. Milleilungen Zool Mus 3:3–98
Stonehouse B (1953) The Emperor Penguin (*Aptenodytes forsteri*, Gray): I. Breeding behaviour and development. HMSO, London
Triche N (2005) "*Aptenodytes forsteri*" (on-line), digital morphology. http://digimorph.org/specimens/Aptenodytes_forsteri/juvenile/whole/. Accessed 25 June 2020
Vanden Berge JC (1999) Modelling the avian cervical vertebral system: structure, function, and phylogeny. In: Adams NJ, Slotow RH (eds) Proceedings of the 22nd international ornithology congress, Durban. BirdLife South Africa, Johannesburg, pp 69–81
Virchow H (1931) Wirbelsäule und Bein der Pinguine. Morph Jb 67:469–565
Watson M (1883) Report on anatomy of the Spheniscidae collected during the voyage of H.M.S. Challenger. In: Murray J (ed) Report. Zoology 7, pp 1–244
Wienecke BC, Robertson G (1997) Foraging space of Emperor Penguins *Aptenodytes forsteri* in Antarctic shelf waters in winter. Mar Ecol Prog Ser 159:249–263
Winkler DW, Billerman SM, Lovette IJ (2020) Penguins (Spheniscidae), version 1.0. In: Billerman SM, Keeney BK, Rodewald PG, Schulenberg TS (eds) Birds of the world. Cornell Lab of Ornithology, Ithaca. https://doi.org/10.2173/bow.spheni1.01
Zusi RL (1962) Structural adaptations of the head and neck in the Black Skimmer. Publ Nuttall Ornithol Club 3:22–25